

FINAL ENGINEERING PROJECT REPORT

submitted to

The ME 450 Design & Manufacturing III Class

University of Michigan

Upper Limb Terminal Device with Force and Position Feedback

Team 18

Louie DeJonge

Leroy Hansen

Jackie Herriage

Eric Krieg

Sponsor and Section Instructor

Brent Gillespie

Assistant Professor of Mechanical Engineering

University of Michigan

Co-Sponsor

Alicia Davis, MPA, CPO, FAAOP

Orthotics and Prosthetics

University of Michigan Health Systems

Mentor

Jeremy Brown

PhD Pre-Candidate of Mechanical Engineering

University of Michigan

TABLE OF CONTENTS

EXECUTIVE SUMMARY	3
ABSTRACT.....	4
PROBLEM DESCRIPTION.....	4
BACKGROUND	5
REQUIREMENTS AND ENGINEERING SPECIFICATIONS	9
CONCEPT GENERATION.....	10
DETAILED ANALYSIS	12
FABRICATION AND ASSEMBLY	21
PROJECT VALIDATION.....	26
DESIGN CRITIQUE	28
CONCLUSION.....	29
ACKNOWLEDGMENTS	29
REFERENCES	29
APPENDIX A.....	31
APPENDIX B	32
APPENDIX C	34
APPENDIX D.....	38
APPENDIX E	42
APPENDIX F.....	43

EXECUTIVE SUMMARY

Research advances in upper limb prostheses in the last decade must be evaluated in light of user preferences concerning commercial prosthetics: many amputees prefer body-powered over myoelectric prostheses due to the direct mechanical feedback provided by body-powered devices. Myoelectric prostheses allow the user to open and close their prosthetic hand using pickups on their skin that detect muscle contractions in their residual limb. These myoelectric prostheses simulate the mechanical properties of the human hand, however, they do not provide sensory feedback for an amputee to fully interact with the environment. Our task is to integrate sensors to a mechanical gripper to provide feedback that can be used in a research program aimed at enhancing sensory feedback for prosthetics.

A previous ME 450 team attempted a similar, related project in the Winter of 2009. Their terminal device provided force feedback but the motor torque did not provide enough force to grasp objects with a large range of stiffness. After experimentation with this device, Professor Gillespie has tasked our team to focus on the terminal device to provide a system with force and position feedback for further experimentation. A more robust, commercially available prosthetic gripper has been donated to the team. The gripper is capable of producing a gripping force of 90 Newtons, which will allow for experimentation of a wider stiffness range.

Using concept generation techniques, the team moved forward with the position and force sensing solutions. Due to the numerous gear systems in the donated gripper, the system has significant backlash, which we anticipate will make closed-loop control difficult. Thus, the position sensing solution of recording the position of a single digit with an optical encoder will be utilized. Collocated sensing will be used to characterize the position of the system by obtaining the position at the digit by optical encoder and the position at the motor by purchasing a Micromo motor with encoder. The force sensing solution has been focused to develop a digit load cell. Through completion of detailed analysis and optimization of the load cell structure, we will proceed to manufacturing and assembly. The assembly process of mounting strain gauges will require attention to the circuitry and delicate application. The assembly plan is to utilize the half or full Wheatstone bridge configuration to obtain the output voltage difference while the digit is under load. The manufacturing and assembly process will be an iterative process to ensure the highest quality and performance through calibration and then validity testing with foam samples of 4 stiffness values.

Acknowledging the status of the products of the previous team, such as the low force control and low motor torque, we worked with our sponsors to develop design requirements and engineering specifications. Our project is much narrower with a specified goal of providing meaningful force and position feedback on an experiment ready device. We anticipate many challenges in our project mostly concerning the load cell optimization, thus we plan to manufacture numerous iterations with ample testing time. We are required to have a safe, experiment ready, working prototype by April 15, 2010 which can be used by an able-bodied person or amputee to collect data. The prototype must facilitate easy calibration and provide force feedback to the residual limb.

ABSTRACT

Current myoelectric prostheses lack the ability to provide sensory feedback, forcing amputees to rely solely on visual feedback. We have developed a prosthetic terminal device capable of relaying grip force back to the touch (haptic) receptors on the amputee's residual limb. Our device is elemental to an experimental apparatus to test hypotheses in the value of haptic feedback. Our terminal device interfaces with the amputee's residual limb and will be activated by electromyographic (EMG) signals. The prototype will be used in experimentation to test an amputee's ability to distinguish object stiffness using haptic cues, in the absence of visual and auditory cues.

PROBLEM DESCRIPTION

Our team is tasked to design a method of sensory substitution using haptic display so myoelectric prosthetic users can sense the mechanical properties of an object without the need for vision. Currently, there is no way for a prosthetic user to know or sense an object without visual or auditory cues. Under the guidance of our sponsor Professor Brent Gillespie and our co-sponsor Alicia Davis, we will integrate sensors to a donated Otto Bock prosthetic terminal device. The sensors will provide a feedback signal which will then be transmitted to the exoskeleton to be used as a haptic display.

In the context of upper limb prosthetic devices, sensory substitution is a term that describes the process of using a motorized device to a different area of the body to substitute the sense of touch. This is pertinent to our project since our finished terminal device will include integrated sensors that provide the signals for force feedback and sensory substitution.

Professor Gillespie is conducting experiments to test the hypothesis that sensory feedback is feasible to distinguish the stiffness of various objects in the gripper. The experiment will be set up so that the user does not receive visual or auditory cues from the gripper. The user provides the electromyographic signals required to actuate the gripper. The gripper will be placed on a table or in a stand. Foam blocks of various stiffness will be placed in-between the gripper digits in random order and the user is prompted to select which foam block has been placed in the gripper based on haptic display they receive from the exoskeleton. It is important to understand that the results of the experiment are based solely on the user's ability to distinguish between object stiffness and does not fully encompass the amount of information the user is able to comprehend or whether there is a better haptic display.

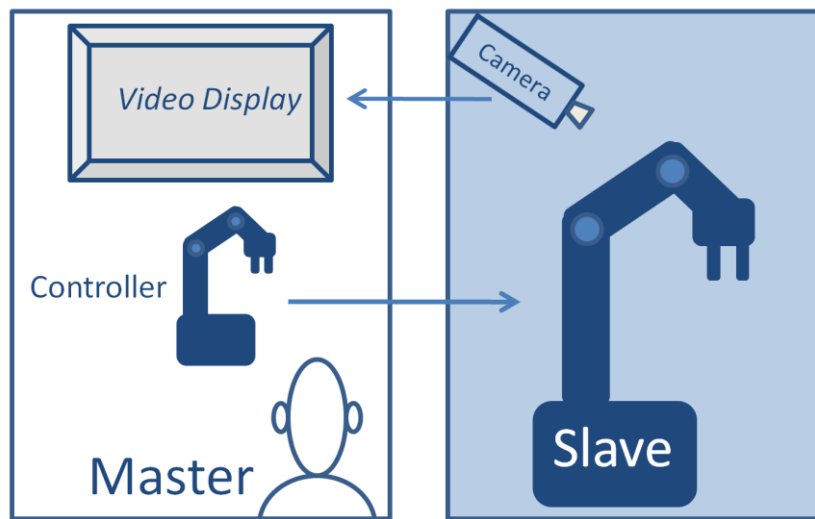
The experiments performed using a previous ME 450 team's terminal device led Professor Gillespie to speculate that a haptic display gives a user the sensory feedback necessary to detect objects in the terminal device without visual monitoring. Deficiencies in the terminal device hindered further testing since the motors on this terminal device struggled to grasp even very soft foam blocks, which limited further testing. Using what was learned from the previous team, our team will now work on a very focused project of improving the feedback supplied by the more robust terminal device. Our re-designed terminal device will meet the needs of an experiment ready prosthetic terminal device equipped with sensory feedback and mounting fixture to be available at or before the Design Expo on April 15, 2010.

BACKGROUND

The aim of this research is focused on gaining a clear and concise understanding of haptics and the motivation behind providing sensory feedback from a terminal device. The most effective way of understanding haptics is to put it into the context of teleoperation. A teleoperator enables a user to use a master device to control a slave device. In a so-called bilateral teleoperator, the master receives feedback from the slave as the slave interacts with the physical world around it and displays that feedback to the user in the form of interaction forces.

Controlling the Slave While teleoperating, the master is isolated from the slave and can control the slave through a variety of ways such as, but not limited to, myoelectric control.² The teleoperating schematic, in Figure 1, portrays the concept of a master controlling the robot slave through the controller. The slave relays back the feedback to the master by the video displays.

Figure 1. Teleoperating schematic



For the purpose of our project a myoelectric control is to be implemented to control the terminal gripping device. A myoelectric device operates electrically by use of EMG electrodes and a small battery. The electrodes are capable of sensing the electric potential that is present when a muscle is contracting. The EMG electrodes are placed in the prosthetic arm adjacent to each other to sense the proper muscle groups involved in gripping. The EMG electrodes are very sensitive and will not operate the terminal device effectively if they are not properly positioned.

The Slave The current terminal device, or the slave, designed by the previous ME 450 Team is seen in Figure 2 on page 6. This two digit gripper featured two servomotors with an encoder. This motor was not able to provide the required torque to apply a sufficient force at the gripper digits. This insufficient gripping force inhibited the device to grasp objects, even a rectangular piece of dense foam.

Taking into account the issues with the current gripper, we explored mechanical grippers that are currently on the market. The i-LIMB by Touch Bionics is one of the top of the line myoelectric prostheses on the market with close to full range of motion, incorporates human hand

characteristics of size, weight, and aesthetics³. The myoelectric controlled prosthesis is a non-invasive device which the amputee controls by residual limb muscle contractions. The speed of the muscle contractions correlates to the speed the hand grasps objects. Other prosthetic terminal devices on the market which are commonly preferred by amputees are the body powered prostheses. A body powered prosthesis arm features a shoulder harness which translates the shoulder movement to the movement of the claw³.

Figure 2. CrustCrawler Robotics Gripper³



After meeting with Alicia Davis, we researched the two mechanical grippers manufactured by Otto Bock, as seen in Figure 3. The DigitalTwin features fast opening/closing speeds, has three digits similar in weight to a human hand and a covering to add aesthetic appeal. The Greifer DMC VariPlu features the combination of high maximal grip force and designed for precise control, thus was eliminated for further work due to the design of the experiment⁴.

Figure 3. Otto Bock Myoelectric System DigitalTwin, left, and Greifer DMC VariPlu, right⁴.



Human skin contains different sensory receptor such as pressure, heat, and pain, which transfer electrical signals through the nervous system to the brain. An amputee using a mechanical gripper is not equipped with these sensory receptors to provide this information to the brain. For the purpose of the slave that is to be used in conjunction with a haptic exoskeleton, only the concept of force, or contact with an object will be incorporated. Upon the completion of our project, our team will have incorporated sensors to a fabricated terminal device to be used as the slave. These sensors will provide meaningful and accurate signals that can then provide feedback to a haptic display.

The Haptic Display of Teleoperating The feedback the master receives from the slave is the haptic display which can take the form of many different stimuli. For the purpose of Professor Gillespie's experiment, the terminal device is to be integrated into an exoskeleton that will be

used by an able bodied user, or a trans radial amputee. Professor Gillespie and others are currently modifying the exoskeleton. The exoskeleton will receive signals from the slave and provide a form of haptic feedback to the user. The current system uses a haptic display of varying torques about the elbow of the user depending on the strength of the signal sent by the sensor. The strength of the sensor signal is based on the amount of strain the sensor picks up.

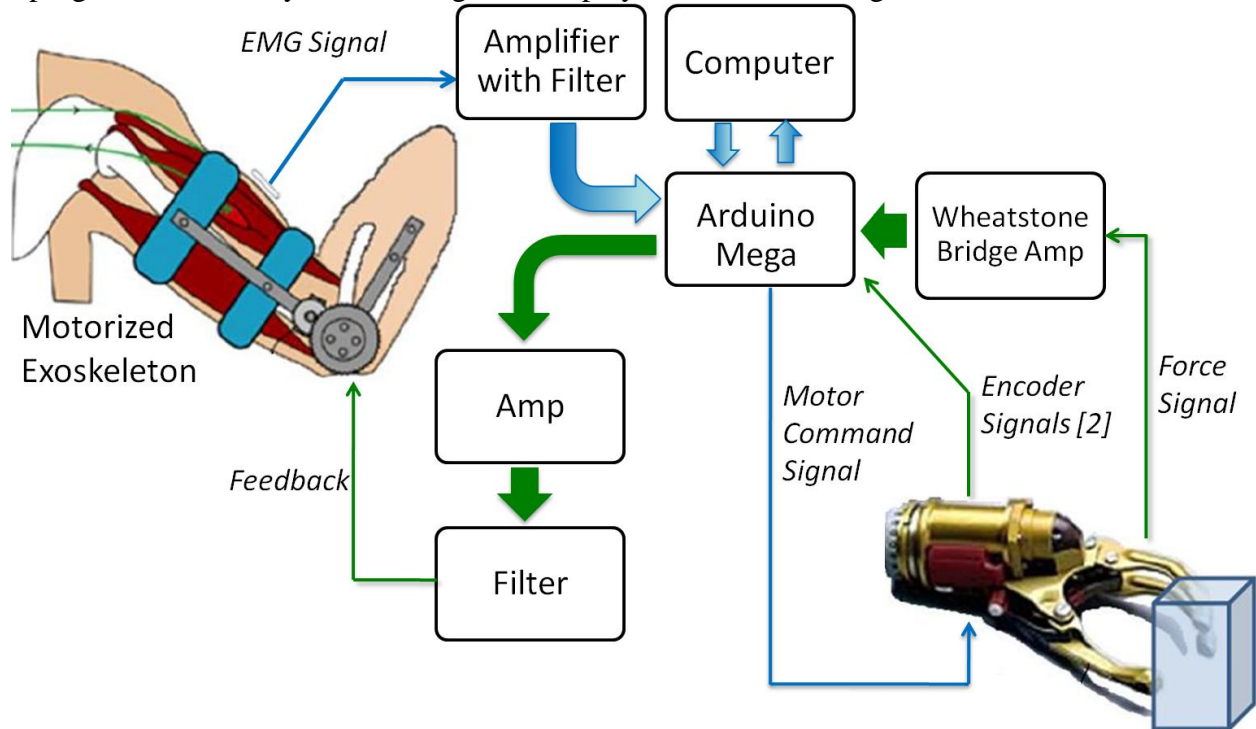
The Cognitive Load of Teleoperating: *Experiment Motivation* The primary concerns that exist within teleoperating and the area of haptics are the impact the haptic display will have on the user's cognitive process and the amount of information the user is able to process. For teleoperating to be effective, it must be proven that the user can interpret the signals received from the haptic display as a result of the slave interacting with its environment. The idea that users of haptic displays are able to recognize, organize and understand sensations received is still in the experimental stage.

To measure the cognitive load, or the amount of information the human brain is able to process effectively, Professor Gillespie has developed an experiment to assess the brain's ability to discern between varying amplitudes of a haptic display. Figure 4, on page 8, shows the experimental setup with the flow of information. In the experiment, the user is connected to the terminal device via EMG electrodes and is fitted with the exoskeleton apparatus. The EMG signal is amplified with a filter to the data acquisition (DAQ) which emits a signal which is amplified and filtered to supply an input voltage to the terminal device motor. This motor command signal then actuates and controls the terminal device. The force and position at the device are relayed to a computer via the load cell and collocated position sensors.

The user, or master, is completely isolated from the terminal device, or slave, and labeled objects of varying mechanical properties are then placed parallel to the device digits. The user is prompted to initiate the movement of the terminal device by flexing their muscles and asked to differentiate between objects grasped under two conditions, with the haptic display off and with the haptic display on. Once the user has selected which piece of foam he/she thinks is in the gripper, they are given verbal confirmation as to whether they are correct. When the haptic display was off, the user had no sensation of what was inside the terminal device and was guessing, which the statistics of the experiment supported. When the haptic display was engaged, the user would initially guess which foam block was in the slave. Through haptic and verbal feedback, the master would learn the correlation between haptic display and the stiffness of the object thus distinguishing between objects of varying stiffness.

From preliminary experiments with the previous terminal device design, Professor Gillespie was able to determine that users were able to correlate the amplitude of the force to different objects to some degree. Thus giving, motivation to our project because the previous gripper lacks the characteristics needed to perform more thorough experimentation to gain more insight into the area of cognitive load.

Figure 4. Experimental setup: User EMG signal is sent as a motion command signal to the gripper; the gripper relays sensed position and force signals through a central data acquisition program; the sensory feedback signal is displayed to the user using the motorized exoskeleton.



We will be testing the device sensitivity to distinguish the stiffness of the foam blocks seen in Figure 5. There are four different foam stiffnesses and each of the samples has identical dimensions.

Figure 5. Temper Foam R-Lite Blocks



Gaps in current technology As a result of gathering important background research, further areas of research have appeared, the most pressing of which is sensor research. While trying to be ambitious by including multiple sensors to improve the function of the terminal device and haptic display, it is necessary to look more closely into the physical specifications of sensors, the cost of sensors and the way in which the sensors output their data. Sensor and control research must be completed to understand how accurately the sensors allow the device to mimic the sensations from a human hand needs to be fully understood. Signal interpretation using microprocessors has been done and will play an integral part in the assembly. The ability for a human to learn the meaning of multiple haptic displays and how these displays correlate to different sensations must be researched in order to ascertain a viable hypothesis. Undecipherable or abundant haptic display may cause user confusion which is undesirable.

REQUIREMENTS AND ENGINEERING SPECIFICATIONS

Understanding our background research and benchmarking, sponsor requirements, and system functions, we have developed engineering specifications and correlating engineering targets for the terminal device.

Sponsor Requirements To begin the process of identifying requirements and developing engineering specifications, we utilized our background research of current state of the art prostheses, haptic and sensor technology. Gaining insight into the field of upper limb prosthetics, we met with our sponsor, Professor Brent Gillespie, who explained the existing state of the gripper device designed by a previous ME 450 Team. He also detailed his expectations for our project highlighting the ability for the device to distinguish between objects of varying stiffness using a haptic display and to be ready for experimentation with amputees by the completion of the term.

Collaborating with Alicia Davis from the UM Prosthetics and Orthotics Center, we were able to learn more of the user needs and learn from her expertise in working with upper limb amputees. Dr. Davis explained the advances which have made in myoelectric prosthesis in the past decade, yet many amputees prefer a body powered shoulder harness due to the analog correlation between shoulder movement and claw grasp and the ability to learn the sensitive feedback control. Dr. Davis has generously provided three mechanical grippers from Otto Bock for our team to work with. Our team will select the gripper which best satisfies the need of mimicking the mechanical aspects of the hand such as having a human like load and grasping capabilities, as well as human like reaction time. Utilizing a developed mechanical gripper will allow our team to focus on incorporating the sensor needs and haptic feedback. Dr. Davis re-iterated as the future of prosthetics being in the area of sensory substitution in myoelectric prosthesis.

Jeremy Brown, Mechanical Engineering a PhD graduate student, will be working on the exoskeleton and was able to provide further details on the design of the previous ME450 Team. He highlighted the previous design's ability to measure force using single point load cells and the linear encoder of the servomotor to determine the gripper position. The torque of the motor was insufficient to compress medium density foam. For our project, he reiterated the need to integrate sensors as well as design a mounting stand for the device to adjust to up to 6 inches off a table surface during experimentation. Jeremy briefly described the experimental setup and the existing computer C++ code which will need modifications with added sensors.

Engineering Specifications After consulting the sponsors of the project and performing thorough background research, we determined product requirements. Developing a QFD, as seen in Appendix A, we identified significant issues as influenced by the determined importance rating. A summary of the key engineering specifications are seen in Table 1 on page 10.

The key difference between current terminal devices on the market and our final goal is the integrated haptic display. The current device, designed by the previous ME 450 team, lacked the motor torque to test forces above 2 N, as determined from the Dynamixel AX-12 DC motor specifications. The pressure/texture requirement is dependent on the capability of a human finger to distinguish small variances. For reference, the force per fingertip for a keystroke is 0.25 N and

Table 1. Terminal Device Engineering Specifications

	Current Terminal Device	Final Goal
Neural Connection		
	Myoelectric Haptic	Myoelectric Haptic
Sensory Capabilities		
Pressure/ Texture	None	0.1 N/fingertip
Force	Deficient (<2N)	40 N
Position	Deficient	1 mm
Power & Actuation		
Grip Force	2 N	90 N
Operating Voltage	10 V	12 V
Opening Width	100 mm	79 mm
Mass	150 g	500 g

a push button is 1 N. The force requirement for a sufficient grip is dependent on the gripping strength of 40 N for weak woman. These force values were obtained from Humanscale, a collection of research values understanding people and their physical attributes, abilities, and limitations⁵. The position of the gripper opening is critical to determining if there is no object in the gripper, thus a 1 mm position requirement will be adequate to determining if there is no object interaction. These engineering targets are also reflective of the sensory capability engineering targets set by DARPA’s Revolutionizing Prosthetics Initiative⁶. The power and actuation requirements are dependent on the product specifications obtained from the Otto Bock System Electric Digital Hand technical product manual. Critical to the sensory capabilities will be the insensitivity to off-axis and shear forces.

CONCEPT GENERATION

We have developed solution concepts to achieve the need of position and force sensing on the terminal device using the concept generation methods of functional decomposition, benchmarking, and brainstorming. To develop a reliable experiment-ready device to test the hypothesis that sensory feedback provides a feasible means for a user to distinguish the stiffness of an object in the gripper, we brainstormed concept solutions. The functional decomposition, seen in Appendix A, clearly identifies the interactions between the inputs and outputs of the system in the form of the energy, material, and signal. This decomposition allowed the team to pinpoint the focus of the project to the force and position sensors.

Position Sensing Concept Unlike the current gripper, with optical encoders, the Otto Bock gripper does not have position feedback which is necessary for experimentation. Our team has decided to use a rotary optical encoder integrated into the gripper at the output shaft of the electric motor. Mounting the encoder at this position will eliminate most of the noise that would be encountered due to gear backlash at the gripper digits. The mounting location is shown in Figure 6 on page 11.

We investigated the rotary optical encoder, S2 Optical Encoder Kit⁷ by US digital. It has a purchase price of \$75.00. The rotary encoder can be integrated into the computer program with

minor modifications. The encoder resolution will be more than adequate for the purposes of the experiment with 2500 counts per revolution (6.94 counts per degree); this equates to be 302 counts or for the operating range of the Otto Bock gripper. Key specifications are located in Table 2. For a more comprehensive list of specifications see Appendix B.

Table 2. US Digital Rotary Optical Encoder

Parameter	Range
Supply Voltage	+5V
Output Voltage Low	0.5 V @ 8mA
Output Voltage High	2.0 V @ -8mA
Supply Current	56mA

Figure 6. Rotary Optical Encoder



Force Sensing Concepts

Single Point Load Cell In order to meet the sponsor’s requirement of measuring the force an object applies when it is placed in the terminal device, the concept design of a single point load cell had been created. A single point load cell, shown in Figure 7 on page 12, has material removed such that when a force is applied to the block, the load cell is allowed to deflect. The geometry of the material removed determines that capacity of the deflection that is allowed and the direction that the load cell deflects. The deflection is allowed in the plane that is perpendicular to the geometry of the material removed. The minimum amount of force required to deflect the load cell, as well as the maximum capacity the load cell is able to withstand before fracturing or permanent deformation occurs, is determined by the amount of material removed and the wall thickness perpendicular to the plan of deflection.

To quantify this deflection and allow for output of some measurable quantity, a strain gauge is strategically placed to deform with the load cell. A strain gauge is made up of a wire that is placed on insulator material so that when a current is placed through the wire, the wire is able to deform, but the object the strain gauge is placed on does not affect the electrical properties of the wire. The strain gauge is placed on the face perpendicular to the plane of deflection and deforms with the load cell. A current is applied to the strain gauge and when the face of the load cell that the strain gauge is placed on is relaxed, the strain gauge will output a voltage that is proportional to the current and resistance of the wire. If the face of the load cell that the strain gauge is placed on is in tension, the strain gauge will stretch. This stretching of the strain gauge increases the area of the wire and the resistance, decreasing the voltage output signal. Conversely, in compression, the gauge length will decrease and increase the voltage output signal. It is through

the conductive and elastic properties of the strain gauge that the force can be measured and then after calibration, the voltage output can be correlated to the amount of force.

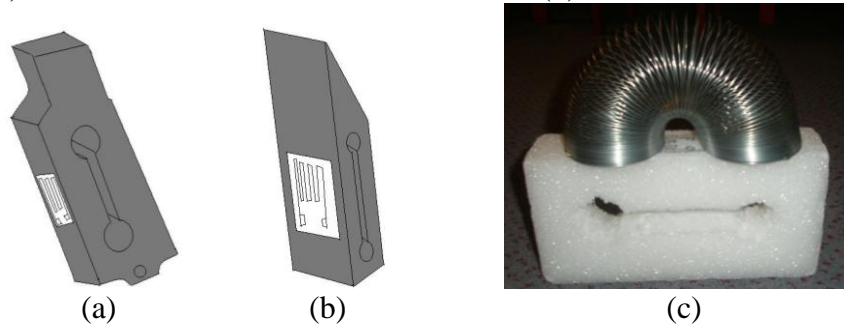
Figure 7. A single point load cell



There are two ways to apply single point load cells to measure the force being exerted on the terminal device from the object within it. Both of these applications will require the removal of the “thumb” digit of the Otto Bock and replacing it with some form of single point load cell. The first application, as seen in Figure 8(a) is to buy a single point load cell and fabricate an attachment and fingertip contact method. The other application, as seen in Figure 8(b) is to design our own load cell and fabricate it on a water jet and mill and mount strain gauges ourselves.

The most important advantage of using load cells is that they wouldn’t be affected by off axis loading. Also, they allow for a direct measurement of force at the contact point of the terminal device. For the purpose of our project, the load cells would require minimal machining and the machining would not be outside the scope of our abilities. The load cells and strain gauges are also relatively inexpensive and would allow for other projects to be pursued as well. On the other hand, the strain gauges have a relatively high resolution of 10% and are affected by ambient factors such as drift and temperature. The strain gauges also require an amplifier in order to power the exoskeleton because the output voltage is so small, but Professor Gillespie is already in possession of one and this would not introduce any cost or too much work.

Figure 8. (a) Purchased load cell with modified ends (b) Fabricated load cell (c) Mock up



DETAILED ANALYSIS

From our concept generation we have selected to manufacture and assemble a single point load cell in the shape of a digit. This section is a detailed analysis of how we will implement our solutions to force and position sensing.

Reverse Engineering In order to incorporate our digit/load cell design into our Otto Bock gripper, our team needs to better understand how the gripper works. There are many aspects of the gripper that need to be characterized, including the gripper digit and drive motor.

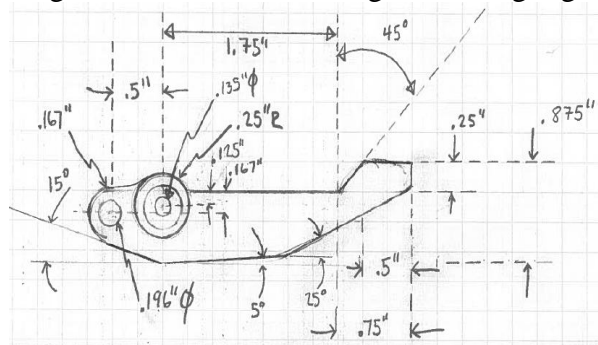
Gripper Digit An accurate and detailed drawing of the existing digit is required as the geometry of the gripper digit needs to be integrated into the design so the digit load cell range of motion is the same as the existing gripper digit. The gripper digit was disassembled in the ME machine shop, a photo of the disassembled gripper can be seen in Figure 9.

After the gripper digit was removed a detailed drawing of the digit was made. The digit drawing was made on graph paper and all dimensions were measured using a vernier caliper (resolution ± 0.0002), an image of the detailed gripper digit drawing can be seen in Figure 10.

Figure 9. Disassembled Gripper Digit



Figure 10. Detailed drawing of existing digit



Design Selection After a discussion with Professor Gillespie and input from others, our team has decided to move forward with the concept of designing a single point load cell. After careful consideration of our knowledge and abilities our team made the decision that the end results of this design selection would give the best force sensing solution possible.

With our design selection complete, we researched common load cell designs to figure out how we could optimize the load cell we will produce. We looked into load cells that had internal geometries as shown in Figure 11 on page 14. We concluded that the dumbbell design as seen in Figure 11c on page 14. will give us the best results for our application. With the geometry that is taken out of the middle it allows for fairly large stress regions directly above and below each circle so that an appropriate resolution can be obtained with the strain gauges. However, the geometry also allows the beam to maintain a large amount of its stiffness so that it does not deform. In our application it could be severely detrimental to the gripper's function if the digit were to deform within the operating loads. This particular design is also optimal for our application due to the way it will deform and create tension and compression regions, as shown in Figure 12 on page 14, which will be used to strategically place strain gauges.

Figure 11. Load Cell Designs

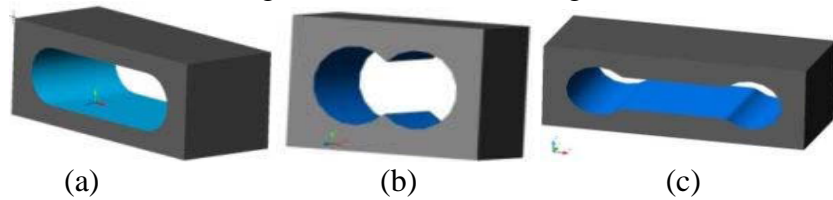
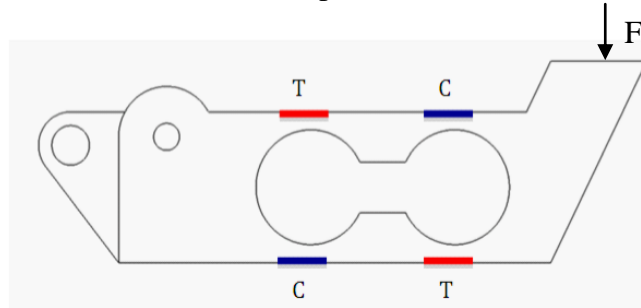


Figure 12. Load Cell tension/compression relation for chosen design.

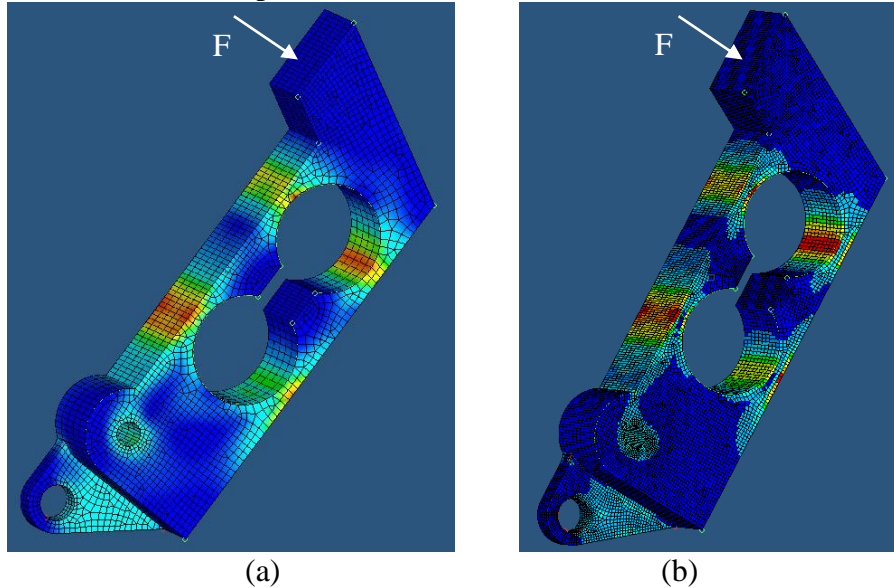


Initial Stress/Strain Analysis After selecting our design we performed calculations to get an estimate of the stresses and strains the load cell will experience. Several assumptions were made to simplify the problem since we were only interested in approximate numbers to ensure that our design was possible and within an acceptable safety factor before we moved further. Some of the simplifications were to assume the neutral axis was down the center of the part and that the geometry beyond the maximum stress point wouldn't affect the calculation to a significant degree. We determined the maximum stress to be 2500 psi and the maximum strain to be 0.025 percent. To determine these numbers we looked at a cross section where we knew the maximum stress would occur as shown in Figure 13 on page 15. Detailed calculations can be seen in Appendix D. These numbers were well within the material and strain gauge properties since the material can withstand strains of 0.5 percent and the strain gauges will not fail with up to 1.0 percent strain^[13]. With the simplifications made these numbers are only rough estimates, but gave us assurance that the design will be feasible.

Finite Element Analysis To better understand the function of the load cell when a load is applied, a finite element analysis, FEA, was undertaken. This was done by importing the geometry of the solid form the CAD model that had already been created, then creating surfaces and elements on the model so that the simulation could be used. The elements were applied to the surfaces so that there were as few inconsistencies as possible and the areas around the suspected highest stress concentrations had more refined elements. The elements were made with the material properties of T6061 Aluminum and were 3D elements such that their entire geometry was defined by the CAD model and number of elements. The two holes that would interface with the existing gripper were constrained in all three degrees of freedom and a 100 N force was applied evenly over the face of the contact area at the end of the model. This simulation resulted in the maximum stress concentration of 7500 psi and 0.075 percent strain. The model was then split so that there were four times as many elements and the model was more refined. The simulation was then performed again and obtained a maximum stress of 7900 psi and 0.080 percent strain. The stress concentrations can be seen in Figure 16. The FEA can be considered valid because there were no inconsistencies from when the model was refined.

The stresses in the high stress concentrations did not increase dramatically and the stress concentrations occurred in the zones that were expected.

Figure 13: FEA models (a) simple stress concentrations and (b) detailed stress concentrations

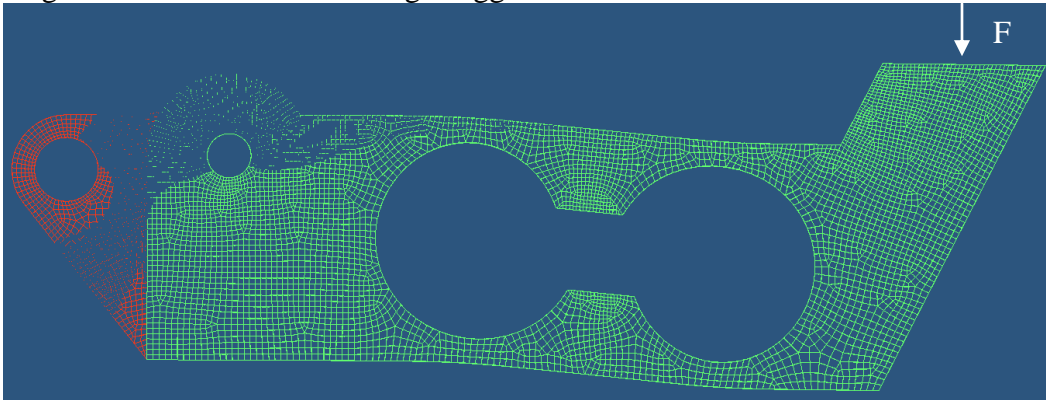


When the load cell is under a 100 N load, the FEA shows that the model only achieves a maximum strain of about 0.08 percent which is much less than the load cell and strain gauges deformation limits. It can be concluded that the load cell will be able to operate safely at a relatively high load and will operate safely at the expected operating loads of the experiment which are expected to be about 5 N to 40 N.

The way the load cell deforms under load is important to understand the areas of stress concentrations as well as the tension and compression zones. Figure 14 on page 16 shows the upper edge of the load cell is split into two zones, one zone in compression and the other zone in tension. This occurs because as the load cell is pushed downwards, the top portion of the left circle contracts which causes material to be “pushed” upwards and makes the upper left edge expand into tension. Conversely, the top portion of the right circle expands, causing material on the right edge to collapse into compression. The bottom portion of the circle reacts in unison to the upper portion. The bottom portion of the left circle must expand to maintain the volume as the upper portion contracts and this expansion of the lower portion causes the bottom edge to be in compression. The lower portion of the right circle contracts as the upper portion expands causing the lower right edge to be in tension. It is these high stress concentrations at the thin walled regions will be utilized to mount strain gauges.

Manufacturing Our gripper design will involve the manufacturing of four parts; the gripper digit load cell, the gripper mounting fixture (Horizontal and Vertical) and the gripper digit load cell pivot shaft. The detailed drawings and manufacturing plans can be viewed in the safety report¹³.

Figure 14: FEA model showing exaggerated deformation of load cell under load



Manufacturing Plans For the purposes of machining, the only materials that will be used that require cutting feeds and speeds are 6061 Aluminum and 1018 low alloy steel. From the Machinery Handbook (page 1044) the cutting speed for end milling 6061 Aluminum is 165 fpm¹⁵. The cutting speed for 1018 low alloy steel (page 1045) is 125 fpm. The formula for the spindle speed in rpm of the cutting tool can be found in the Machinery Handbook (page 1016):

$$N = \frac{12V}{\pi D} \quad \text{Eq. 1}$$

Where N is the spindle speed in rpm, V is the cutting speed per material being machined, and D is the cutting tool diameter. Before any machining can begin a datum must be established using a center finder.

Strain Gauge Assembly Since the transducer behavior can have a very low resolution, the strain gauge system shall be carefully selected and installed. Strain gauges installed on a transducer can be easily calibrated using known physical parameters, for example dead weights. Several criteria were considered when selecting the gauge parameters including gauge width, length, grid pattern, and resistance. The Vishay Linear Dual Grid: Half Bridge gauges, as seen in Figure 15 on page 17, were provided by Professor Gillespie and meet the overall package dimensions to fit on the designed transducer. The gauge resistance of 350 ohms is standard and will provide a measurable voltage divider signal when connected in a Wheatstone bridge configuration, which will need to be amplified.

The strain gauges respond to strain in the direction of the transducer strain and are insensitive to lateral forces. From the FEA analysis, the areas of maximum strain were identified as the optimal location for the strain gauges as rendered in the schematic in Figure 15 on page 17. The Vishay Dual Grid gauges can be arranged as a single gauge by only wiring to the input and output terminals of a single resistor. Under tension the length of the conductor coil increases, causing the resistance of the gauge to increase. Likewise, in compression the conductor coil shortens, causing the resistance of the gauge to decrease.

Strain gauges can be configured in a number of useful electrical circuits; however the Wheatstone bridge is the most basic to measure resistance changes in transducers utilizing four resistors. One possible method for our transducer design is the half-bridge circuitry, as seen in Figure 16 on page 17 in which there are two known resistors and two active resistors arranged in

a full bridge. The two active gauges respond to the tension and compression loads applied with changes in resistance resulting in a voltage divider output. This output is then amplified and calibrated to obtain force. The linearity is best when the amount of resistance change induced from the applied force is small compared to the nominal resistance.

Figure 15. Strain gauge specification and assembly location

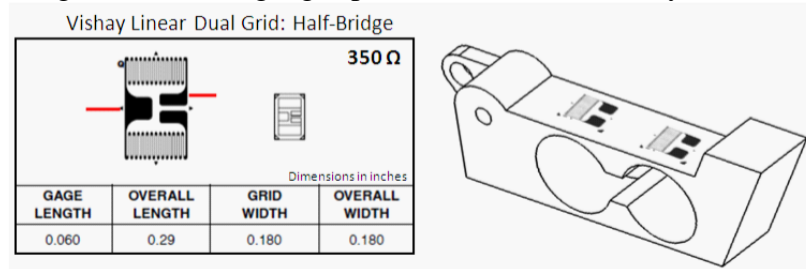
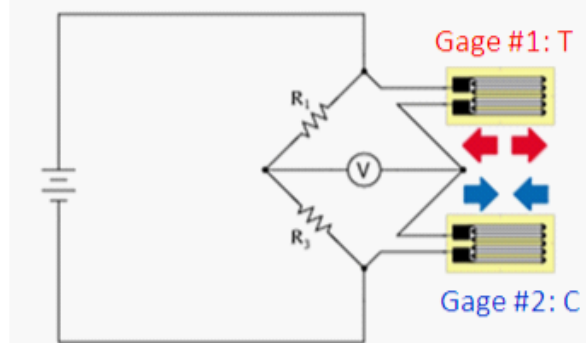


Figure 16. Half-Bridge Circuitry: There are two nominal constant resistors and two active gauge resistors. The resistance change affects the output voltage which is calibrated to force.



To increase the sensitivity of the circuit, a full bridge circuit can be utilized, as seen in Figure 17 on page 18. All four of the arms of the bridge are now active strain gauges and are mounted such that two gauges are in tension and two gauges are in compression. In a full bridge, the resistance change in all four active gauges is ideally equal and the output voltage will be directly proportionally to the applied force.

The mounting procedure for strain gauges is an extremely delicate procedure and our team will be working with Todd Wilber to ensure proper mounting and wiring. We will be following the strain gauge mounting step by step procedure according to the Vishay mounting kit as well as the guide by Measurements Group pages 47-79¹⁶.

In summary, the digit transducer design has been selected as the top design due to favorable factors strengthening the likelihood for project success. The design compactly interfaces with the current terminal device, linearity over a wide range of strains, and the circuit output is resistance which is highly stable over time. This design is limited by the use of an amplifier, due to the low output signals, and the challenges mounting and protecting the transducer strain gauges require further attention and care. These factors are summarized in Table 3 on page 18.

Figure 17. Full Bridge Circuitry: Gauges R1 and R4 are in tension under load and experience the same strain thus the resistance change is the same in the fully active Wheatstone bridge. Gauges R2 and R3 are in compression under load and experience the same strain and same resistance change.

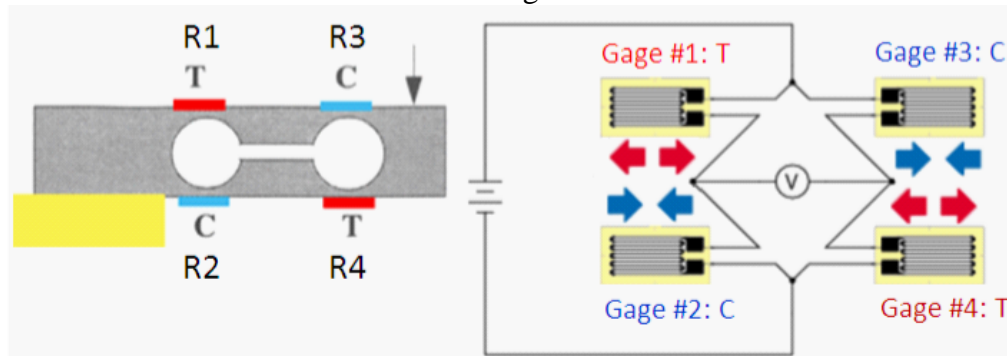


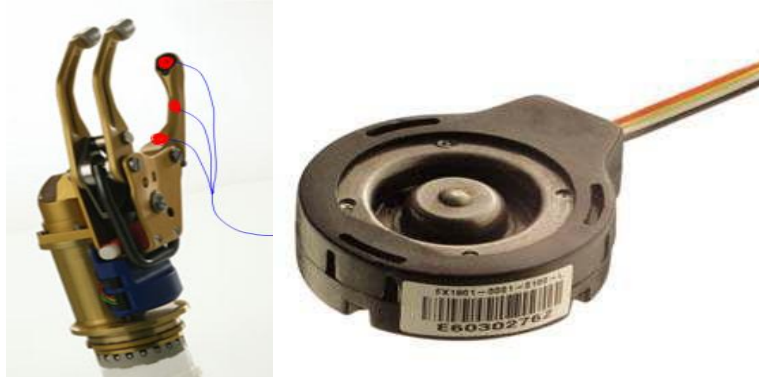
Table 3. Transducer Design Factors

Favorable Factors	Limiting Factors
Small size, low mass	Output signals low, require amplifier
Excellent linearity over wide range of strains	Careful installation of strain gauges required
Highly stable with time	Fragile to impact
Relatively low cost	Protective coating needed to limit moisture effect
Circuit output is resistance change	
Low and predictable thermal effects	
Wheatstone bridge ensures low output noise	

Validation through Variation To validate the selected design, we will implement a plan in which multiple load cells are manufactured. Each load cell will have a different geometry removed from the inside of the load cell that will change the minimum wall thickness and therefore the maximum stress. Strain gauges will then be placed on the load cells and testing will begin. The load cell that allows for the highest voltage difference that corresponds to the highest strain, without deforming the load cell or strain gauges will be selected as the optimal design. This plan is to be implemented because there are many assumptions made and factors that cannot be predicted by hand calculations and FEA. Due to the relatively low amount of manufacturing as well as the availability of materials, this course of action will allow for the optimal design to be selected under real world application and the validation, or invalidation of our design. Both of which will lead to further investigation and understanding of load cells and strain gauges as it relates to our project.

Backup Load Cell Due to the challenges presented with designing and assembling our own load cell, we have sought out a low cost, compression load cell. While the parameters of this load cell meet our engineering specifications and would be easily mounted to the gripper, the contact sensing area limits the performance during experimentation. If we need to pursue this alternative, we will need to evaluate and design a larger sensing area to attach to the compression pin, as shown in the Figure 18 on page 19. Detailed specification of this product can be found in Appendix D.

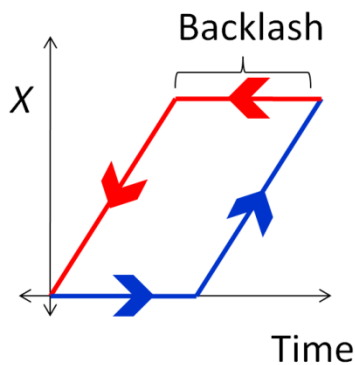
Figure 18. FX1901 Compression Load Cell, 1" Diameter



Position Sensing The Otto Bock gripper does not have position feedback which is necessary for experimentation. After discussions with Professor Brent Gillespie we have decided that the backlash could not simply be ignored. Our team has decided to use a magnetic encoder integrated into the gripper at the output shaft of the electric motor. An optical encoder will also be placed at the pivot point of the load cell digit. Mounting the encoders at these positions will address the noise associated with backlash.

Backlash The Otto Bock gripper has several different gear trains that are utilized in the design to resolve several issues. The existing gripper drive motor is capable of outputting 8000 rpm. In order to reduce the motor speed and increase output torque a planetary gear system is utilized. The rotational motion of the planetary gear reduction output shaft then needs to be rotated 90° , to solve this problem a bevel gear system is used. Finally, a compound spur gear system is then used to transmit this motion and torque to actuate the gripper. All of these gear systems have slack designed into them in order for the gear teeth to mesh properly. This introduces a form of hysteresis into our drive system, Figure 19 below shows a theoretical graph of our gripper motion which shows the backlash.

Figure 19. Gripper Motion Showing Backlash



The backlash can be best described as the flat regions shown in Figure 19, above. The origin on the graph represents the gripper in the open position. As the gripper motor actuates all of the slack in the three gripper gear trains is being reduced until the slack has been taken out, shown by the horizontal blue line. The point where the blue line starts to increase in slope is where the gripper digit encoder actually senses movement. The point where the blue line ends represents

the gripper in the closed position. When the gripper reverses direction to open, the reverse process happens where the slack is removed by the motor before movement is detected. These flat regions in the system make the gripper motion non-linear and difficult to control smoothly.

Collocated Position Sensing There are several different ways to address backlash, the solution that we are planning to pursue is collocated position sensing. This is where we will use two position sensors to properly characterize the gripper backlash. We will use an optical encoder mounted on the digit pivot shaft that will enable us to obtain position with backlash. A magnetic encoder will be directly coupled to the gripper drive motor. The backlash will still be in the system, but with collocated position sensing, we will be able to characterize the backlash and have smooth control of the system electronically.

Digit Load Cell Encoder The rotary optical encoder shown in Figure 20 is the E4 optical encoder by US digital⁷. It has a purchase price of \$33.50. The rotary encoder can be integrated with minor modifications to the gripper¹⁴. The encoder resolution will be adequate for the purposes of the experiment with 360 counts or 1440 pulses per revolution (4 pulses per degree); this equates to be 160 pulses for the operating range of the Otto Bock gripper. Key specifications are located in Table 4.

Figure 20. Rotary Optical Encoder with Mounting Location

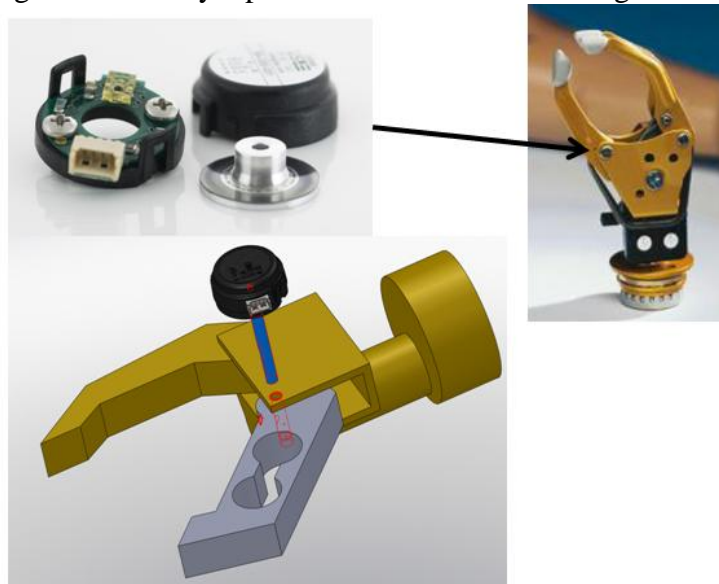


Table 4. US Digital Rotary Optical Encoder

Parameter	Range
Supply Voltage	+5VDC
Output Voltage Low	0.5 V @ 8mA
Output Voltage High	2.0 V @ -8mA
Supply Current	56mA
Operating Temperature	-20 to 100°C

Gripper Drive Motor Encoder Modifications to the gripper drive will be needed in order to fit the gripper drive motor with a position sensor. We have a new motor and encoder on order from Micromo which has an accompanying 512 cycle per revolution magnetic encoder, also from Micromo part number IE2-512. Key encoder specifications can be seen in Table 5. A screen shot showing the intended gripper drive motor/encoder interface can be seen in Figure 21.

Figure 21. Rotary Magnetic Encoder with Mounting Location

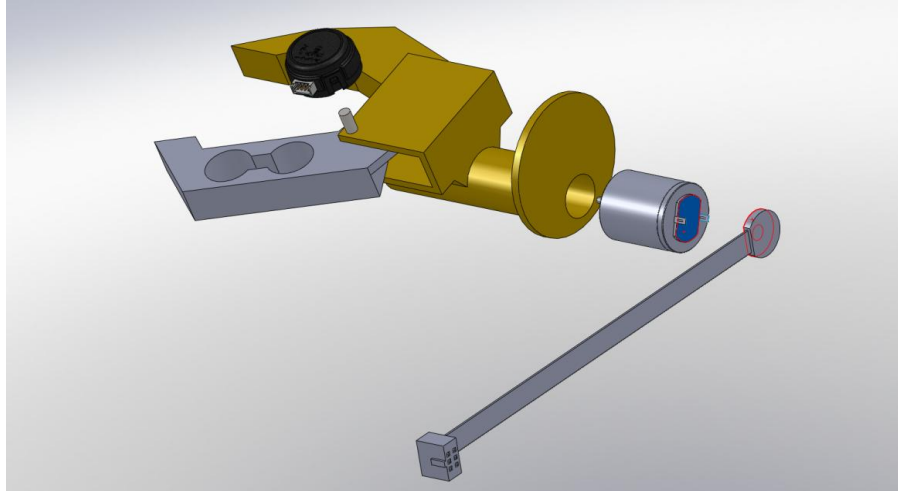


Table 5. Micromo magnetic encoder

Parameter	Range
Supply Voltage	+4.5-5.5 VDC
Output Voltage Low	0.5 V @ 6mA
Output Voltage High	4.5 V @ 5mA
Output Current (Max)	5mA @ 5Vdd

The motor that will be coupled with the encoder is the Micromo 2224T012SR which has the key specifications seen in Table 6. This motor has the same dimensions as the motor previously in the gripper. Data sheets for both the gripper drive motor and the encoder can be viewed in Appendix D.

Table 6. Key Micromotor Specifications

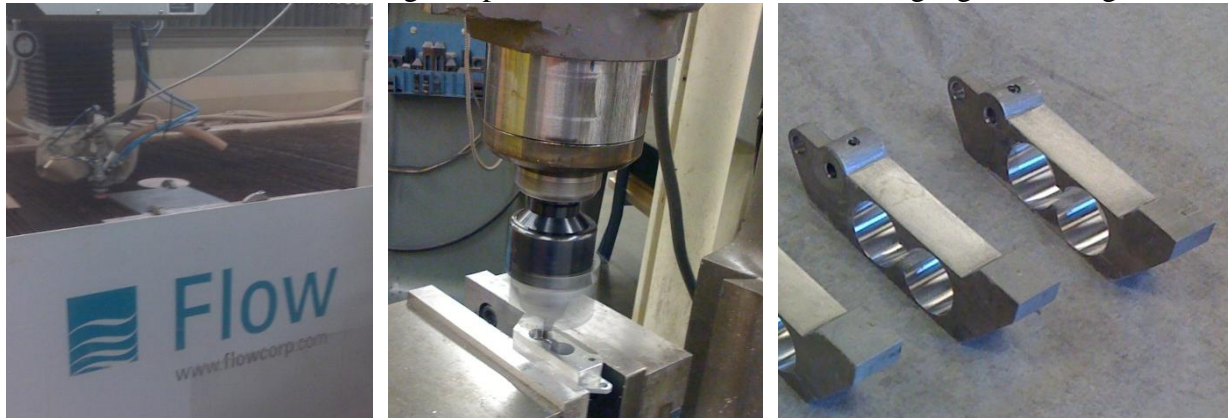
2224 DC Micromotor with encoder	
Nominal Voltage	12 V
No-load Speed	7,800 rpm
Stall current	0.014 A
Encoder	512 count

FABRICATION AND ASSEMBLY

Load Cell Using the CAD models we imported the models to FlowPath, a drawing and flow path software, to upload our design to the Flow Corp waterjet in the Digital FabLab at Taubman College. We cut 5 parts on the water jet to account for manufacturing and assembly errors as

well as to optimize the wall thickness We then used the mill in the ME Machine Shop to bore the binocular hole diameter to the specified diameter and mill the slot to interface the load cell digit with the current Otto Bock gripper. The two parallel surfaces were then prepped for strain gauge mounting by sanding increasing sandpaper grade from 240, 300, 400 and finishing with a 400 grade wet sand. The progression from stock aluminum material to the finished machined part for the load cells are seen in Figure 22, below.

Figure 22. Water jet operations performed on the Flow, binocular designed milled to exact diameter and interfacing completed, surfaces sanded for strain gauge mounting.



We utilized the strain gauge advice and techniques of Todd Wilber, Dr. Tom Bress, and Dr. Brent Gillespie, according to the Vishay strain gauge mounting instructions and strain gauge mounting kit. After surface preparation, we used alcohol to clean the surface followed by cleansing with Conditioner A and Conditioner B. The surfaces were then dried with a clean cloth. 3M removable tape was then sealed on the surface and anchored at one end. The tape was peeled back to the anchored area and a single gauge of the dual grid was set in the desired location, centered at where there is maximum strain. The tape is then pressed to cover the gauge and maintain the gauge location. The tape is peeled back one final time and a light coating of catalyst is brushed onto the underside of the gauge. A small drop of adhesive is placed on 50 % of the gauge and then the tape is pushed from the anchor end to the loose end, while applying ample thumb pressure for one minute over the gauge. The adhesive should be visible spread to all edges of the gauges. We used two different adhesives a two part paste which took 24 hours to dry and the Vishay adhesive which dried in less than 5 minutes. We recommend continuing the use of the Vishay adhesive due to the quick and secure bonding, and also the clear dry appearance, seen in Figure 23 on page 23.

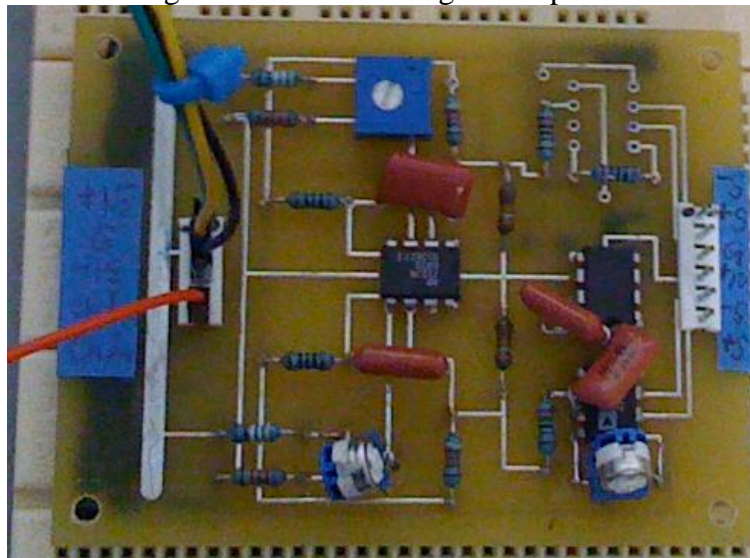
After bonding the gauges, we used flux and solder with a fine tip soldering iron to prepare the solder pads for the wires. We used a gauge wire with 6 strains: red, white, blue, yellow, black, and unwrapped. We paired the red and white, blue and yellow for the input and output pads of each resistor. These leads were then connected to a chip, forming a Wheatstone bridge circuit with the four resistors. Originally, we made a circuit board for the wire leads to connect to a Wheatstone bridge, however John Baker provided us with a chip he designed, allowing the interface to be clean and secure. Figure 23 on page 23 shows the load cell and completed Wheatstone bridge circuitry.

Figure 23. Vishay gauges using mounted, wire soldered, and Wheatstone Bridge assembled.



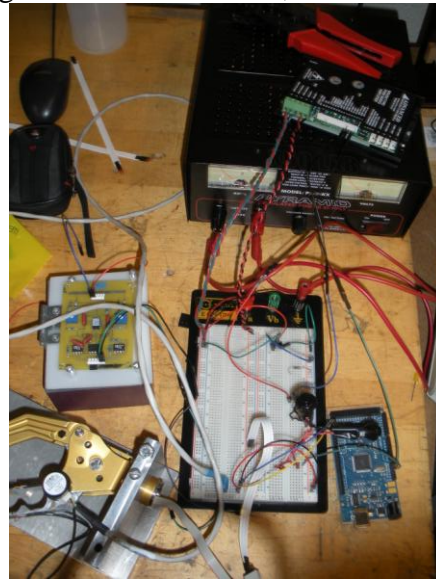
The load cell signals were then connected to an amplifier circuit seen in Figure 24, below. The amplifier uses potentiometers to offset and amplify the Wheatstone bridge output. The amplifier circuit is powered by a ± 10 V Power Supply and outputs from the Channel 1 on the left to the oscilloscope, and in the future through Arduino. The amplifier signal was displayed visually during the Design Expo using an oscilloscope. The initial results indicate the load cell is performing successfully. Further validation results can be seen in the project validation section.

Figure 24. Load Cell Signal Amplifier



Motor and Position Encoders The motor, motor magnetic encoder and US Digital optical encoder are interfaced with the Arduino Mega microprocessor. Following the guidance of Professor Gillespie's tutorials and the assistance of John Baker and Jeremy Brown, we developed Arduino programming code, seen in Appendix C. The connections for the encoders and motor were dependent on the specified pin out provided in the data sheets in Appendix D. Figure 25 on page 24 shows an initial schematic of the wiring between the power supply, servo amp, Arduino, breadboard, and motor. The motor is controlled by switches which change the rotation direction, thus controlling the opening and closing of the gripper.

Figure 25. Setup controlling motor with switches, Arduino Mega, and 15 V power supply.



Final Assembly After the electrical setup was finalized, the new motor and new load cell were integrated with the gripper. The replacement motor featured increased power capacity of 12V and a magnetic encoder. The US Digital Optical Encoder is mounted to the digit pivot shaft. The load cell digit interfaces well with the Otto Bock DigitalTwin. An exploded view of the force sensing prosthetic hand can be viewed in Figure 26. The device is then interfaced with the experimental clamp. An amputee user can interface with the experimental setup easily with the appropriate quick release wrist mechanism. The entire experimental setup is demonstrated in Figure 27, on page 25.

Figure 26. Exploded View of the re-engineered Otto Bock DigitalTwin.

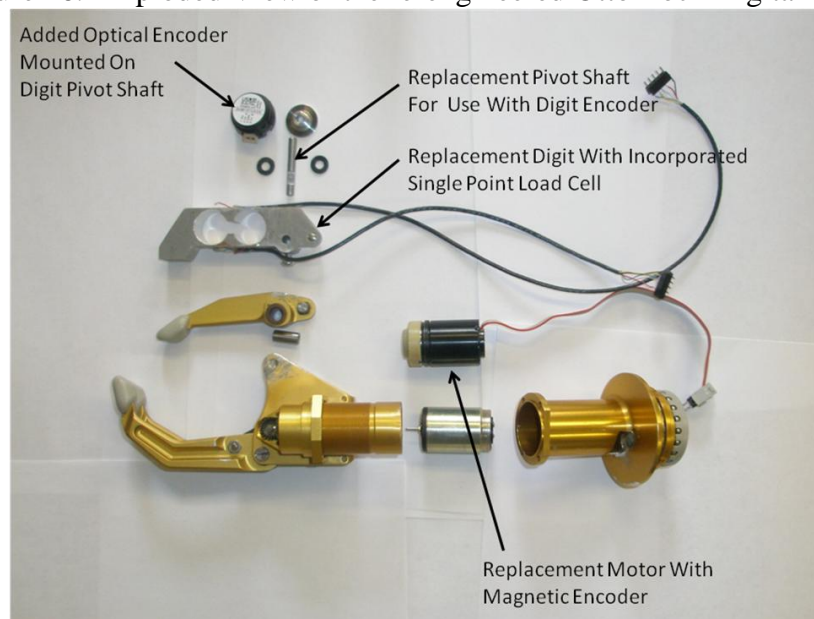


Figure 27. Entire experimental setup. The user is isolated from the terminal device controlled by EMG signals. The force and position sensing signals at the gripper are processed and then relayed back to the user by the haptic display brace.





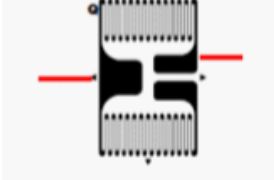
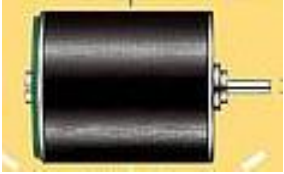
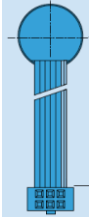

FINAL DESIGN

The final design of our prototype has been developed and is in working order as we intended following our sponsor requirements and engineering specifications. A detailed picture of the final design is shown in Figure 26, page 24. We were able to get our prototype working using a rough system incorporating Arduino software. Further modifications to the system will need to be made before actual experimentation with volunteers, however, the current system was suitable for demonstration purposes.

We have programmed the gripper to open and close using push buttons or the EMG signals. We were able to receive signals from the US digital optical encoder for position sensing of the load cell digit. The encoder counts accurately as it opens and closes, however, we were unable to receive meaningful signals from the magnetic encoder on the new Micromo motor. Using our single point load cell design we were able to amplify the voltage signals coming from the strain gauges and view them on an oscilloscope. In actual experimentation these signals will be used with a haptic display as opposed to the oscilloscope. When the load cell comes into contact with something we were able to view a voltage difference, which can be related to a force through calibration.

The major components in our device can be seen in Table 7, on page 26. Further engineering drawings of components can be found in the safety report. Further information on smaller components and a bill of materials can be found in Appendix D. The cost of the project including donated parts was \$325 (not including the Otto Bock gripper) with a cost to the University at \$154.

Table 7. Final Design Components

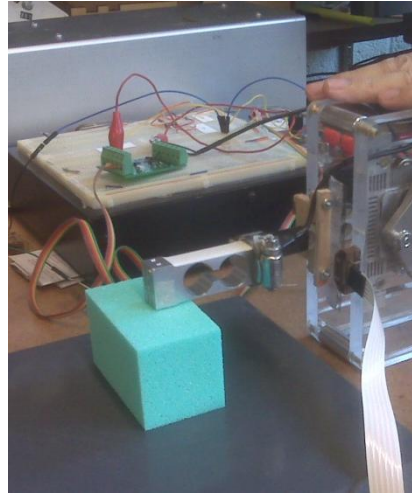
Part Number	Part
Otto Bock Myoelectric System Digital Twin	
Load Cell Digit	
Vishay dual grid strain gauges	
2224 DC Micromo Motor	
IE2512 Micromo Magnetic Encoder	
US Digital E4 Optical Encoder	

PROJECT VALIDATION

After purchasing the Ryolan R-Lite therapeutic foam block variety pack, we setup a plan to calibrate the force readings displayed at each foam stiffness. Using another force sensing setup, Figure 28 on page 27, in Professor Gillespie’s lab, we measured the load, deflection position, and time. The experimental results can be found in Appendix C. The results experimentally

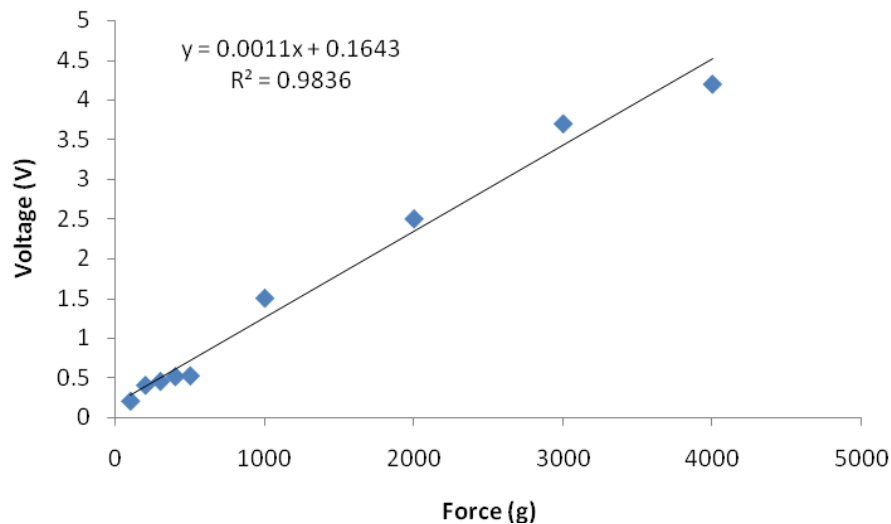
confirmed the range of stiffness to be between 5 N – 15 N from the softest foam (yellow) to the stiffest (green).

Figure 28. Foam stiffness measured using calibrated setup.



Testing is necessary to validate our design and ensure that the final product satisfies our engineering specifications and sponsor requirements. The method of validation used was to perform a simple calibration using a fish scale and oscilloscope while the gripper was in its operational state. With the oscilloscope zeroed and the gripper in its resting state, the fish scale was hooked to the end of the digit and pulled away from the gripper to place the back of the digit in compression and the front in tension. This change in stress will result in an increase in the voltage which can then be read from the oscilloscope. The load applied was in grams and there is considered to be no effects due to gravity because the force was horizontal and the strain gauges were only measuring forces in the plane perpendicular to the gravitational force. The calibration curve can be seen in Figure 29.

Figure 29: Calibration curve for validation of gripper



The calibration curve is nearly linear, a desired design factor because it allows for simple calibration and interpretation of results. Further calibration needs to be done once controls have been put in place to command the motor to close the digit to a designated position. Once this has

been done, the foam blocks can be calibrated as they will be compressed the same amount, but due to the varying stiffness of the foam, the amount of force and subsequent voltage output of the digit will be different. We expect the calibration curve to be similar to that of the foam block calibration curve seen in Appendix C with the appropriate gain and offset applied to the amplifier.

DESIGN CRITIQUE

While adequate time was spent in planning, producing and validating our final design, it is not without its flaws. The most notable flaw of the final product is the lack of refinement in the wiring and electrical connections. Due to our lack of experience in soldering and lack of resources to produce quality crimps, headers and other electrical connections, the electrical system is very unstable and considerable time needs to be put into strengthening these connections. Another flaw of our design is the amount of friction introduced into the system. The space where the digit is placed between the walls of the existing gripper does not have enough room to allow the digit to move freely. In order to resolve this issue, the digit could be redesigned to be thinner at this section and bearings or a sleeve could be used to reduce friction. While it is advantageous to have an optical encoder placed on the pivot shaft of the digit for closed loop control, there is no place to securely attach the nonmoving housing to prevent off axis movement. This could result in poor accuracy of readings and the need to constantly monitor and adjust the encoder to ensure accuracy. To resolve this issue the housing must be made static by utilizing the other set screw hole to affix the housing to another static part of the gripper. Another flaw of the final design is the motor that was placed in the gripper. The motor is not the correct length for the housing and it is difficult to ensure that the entire output capabilities of the motor are being transferred to the gear system that drives the digits. This can be remedied by adjusting the screw cap that holds the motor in place or using a spacer in between the screw cap and the motor.

RECOMMENDATIONS

The final state of the product is functional and robust, the overall design of our project meets and exceeds the engineering and sponsor requirements, but there is always room for improvement. In order to allow the system to be more reliable and portable, the wiring and electrical connections should be strengthened so that there are no loose connections and the device will be reliable. The mechanical system can be improved by fitting the pivot shaft with bearings or a sleeve to reduce friction and allow the digit to move more freely. The optical encoder should be secured to a static part of the system so that the readings are accurate and repeatable. The motor must be prevented from moving away from the interface with the planetary gears by adjusting the screw cap holding it in place or placing a spacer between the screw cap and the motor such that the motor will have a strong connection to the gear system. The controls of the system must also be improved to allow for experimentation. At this time the only reliable way to control the device is with a push button system and the magnetic encoder on the motor is not outputting accurate information. In order to make use of the full capacity of the gripper, this encoder must be made to work and controls need to be put into place so that the motor can be commanded and

the placement of the digit is known. Once the control of the system is better initialized the system can be further calibrated and integrated into the current haptic display. Once these issues and recommendations have been addressed, the gripper will be ready to be used in experimentation for Professor Gillespie.

CONCLUSION

Professor Gillespie is testing the hypothesis that haptic feedback is the most useful form of sensory substitution. Our team was tasked with the project to create a more robust terminal device that incorporates force and position feedback. After we were donated an Otto Bock prosthetic gripper force and position were deemed the primary focus for the design solution of this project. To create a smooth operating closed-loop control system our team incorporated the idea of collocated position sensing. This means that we included an encoder to measure the digit location as well as an encoder to measure the motors position. This is done to characterize the backlash in the system so that we know the digits position in relation to the motor. To address the issue of force feedback our team designed a new thumb digit for the Otto Bock prosthetic gripper that incorporated a single point load cell design. Using knowledge we obtained from current load cell designs we were able to design and manufacture the load cell to be similar size and performance as the original thumb on the Otto Bock gripper to maintain the gripper's function. We placed strain gauges in particular locations on the load cell and wired them in a Wheatstone bridge configuration. Using this form of wiring we were able to read a voltage difference as the strain gauges are deformed. By creating a calibration curve we were able to relate this voltage difference to a particular force. Our device works as we would expect and with some modifications to the control system will be ready for use in Professor Gillespie's experiment. Our device has incorporated all of our sponsor's requirements and will allow Professor Gillespie to perform experimentation that will allow for advances to increasing the standard of living for trans radial amputees by integrating the sense of touch to their prosthetics, as well as other areas of research including the idea of teleoperating.

ACKNOWLEDGMENTS

Special thanks to Professor Gillespie, Alicia Davis, Jeremy Brown, John Baker, Todd Wilber, Taubman College: Fab Lab, Bob Curry, and Marv Cressey, and Professor Kurabayashi.

REFERENCES

- [1] Fuhrman, Richards, Straub, Wiley. "Smart Prosthetics for the Upper Extremity" April 2009.
- [2] Gillespie, Brent. Lecture6_MechatronicsME450W10.pdf. February 3, 2010.
- [3] Performance of Above Elbow Body-Powered Prostheses in Visually Guided Unconstrained Motion Tasks . Joseph A. Doeringer and Neville Hogan . IEEE TRANSACTIONS ON BIOMEDICAL ENGINEERING, VOL. 42, NO. 6, JUNE 1995
- [4] Otto Bock. <http://www.ottobock.com/> January 18, 2010.

- [5] Niels Diffrient, Alvin R. Tilley and Joan Bardagjy. "Humanscale". Henry Dreyfuss Associates, MIT Press.
- [6] REVOLUTIONIZING PROSTHETICS PROGRAM. DARPA Press Release. February 2008. http://www.darpa.mil/Docs/prosthetics_f_s3_200807180945042.pdf
- [7] US Digital. S2 Rotary Optical Encoder . <http://www.usdigital.com/> February 10, 2010.
- [8] Honeywell. AQMLT Series Linear Potentiometer. <http://www.newark.com/honeywell-s-c/aqmltr5n00750fc/linear-sensor/dp/30C4593> February 10, 2010.
- [9] National Instruments. NI DAQ Card 6062E2 Bit Multifunction I/O. <http://www.ni.com/> February 10, 2010.
- [10] McMaster-Carr. Precision Compression Spring 94125K541. <http://www.mcmastercarr.com/> February 10, 2010.
- [11] Omega. Economical, OEM Style Single Point Load Cells. www.omega.com . February 15, 2010
- [12] Analog Devices. AD22151G: Linear Output Magnetic Field Transducer. www.analog.com. February 15, 2010
- [13] Aliyari, M, et. all. Load Cell Design and Construction with Fault Detection by Probabilistic Neural Network. March 10, 2010.
- [14] Team 18 ME 450 Safety Report, ver. 1.2. March 21st, 2010.
- [15] Oberg, Erik. Machinery's Handbook: a Reference Book for the Mechanical Engineer, Designer, Manufacturing Engineer, Draftsman, Toolmaker, And Machinist. 28th ed. New York: Industrial Press, 2008.
- [16] *Strain Gauge Based Transducers: Their Design and Construction.* Technical Staff of Measurements Group, Inc., Raleigh, North Carolina. 1988.

APPENDIX A

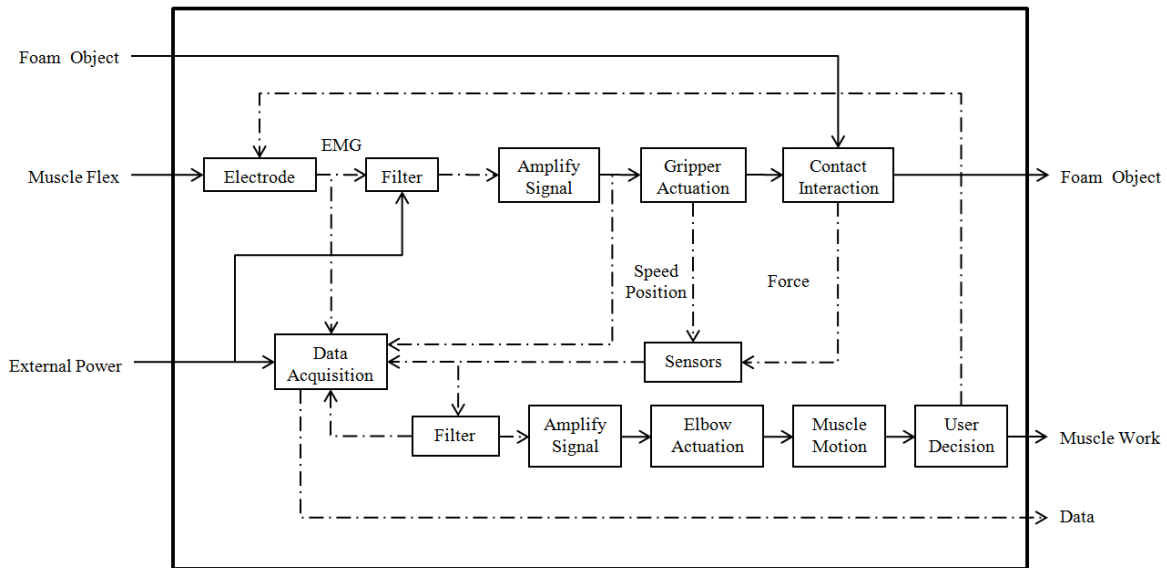
System QFD

		Project: Upper Limb Terminal Device													Date: Jan 21, 2010					
1	Force (+)																			
2	Reaction Force (+)	9																		
3	Angle (+)	-3	-9																	
4	Length (-)	0	-9	9																
5	Weight (-)	0	-9	-9	3															
6	Speed (+)	0	-9	-9	0	-9														
7	Voltage (-)	0	-9	-9	3	9														
8	Amperage (-)	0	-9	-9	3	9	9													
9	Reaction Time (-)	-3	-3	0	9	0	9	9	9											
10	Failure Load (+)	0	0	-3	-9	-9	-9	-9	-9											
11	Torque (+)	0	3	3	9	3	3	3	0	9										
12	Number of Force Sensors	3	0	3	-9	0	0	-9	9	3										
13	Number of Position Sensors	-9	-9	9	9	3	9	3	3	0	-9	-9								
14	Number of Pressure Sensors	9	9	-3	-9	-3	-9	3	3	-9	9	-9	9							
15	Number of Cycles (+)																			
16																				
17																				
18																				
19																				
20																				

Customer Needs	Customer Weights (1-10)	Technical Requirements											Customer Opinion Survey							
		Force (+)	Reaction Force (+)	Angle (+)	Length (-)	Weight (-)	Speed (+)	Voltage (-)	Amperage (-)	Reaction Time (-)	Failure Load (+)	Torque (+)	Number of Force Sensors	Number of Position Sensors	Number of Pressure Sensors	Number of Cycles (+)	1 Poor	2 Acceptable	3 Excellent	
1	Grab an object	8	3	3	3	3	3	3	3	3	3	3	3	3	3	3				
2	No way to tell if an object is hard or soft	3	3	3																
3	Needs to look good	5			3	3														
4	Cannot sense position	7			3	3			3	3										
5	Needs to grip various geometries	3	3	3	3	3	3													
6	Needs to be light weight (Same as human hand)	6	3	3	3	3	3	3												
7	Needs to open and close fast	6			3	3	3	3												
8	Needs to use a small battery	5	3			3	3	3	3	3	3	3	3	3	3					
9	Know how much force gripper is applying	3	3	3	3	3														
10	Needs to be durable	5	3	3	3	3			3	3	3	3	3	3	3					
11	Needs to detect pressure	4	3	3					3	3	3	3								
12	Needs to last	7	3	3	3	3	3	3												
13	Full motion ability	8			3	3	3													
14																				
15																				

Technical Requirement Units	N	N	Degrees	m	kg	mm/s	V	Amp	Seconds	Mpa	Nm	#	#	#	#
Technical Requirement Targets	133.450	133.450	90.000	0.060	0.300	0.300	7.000	0.100		#####		2.000	1.000	2.000	
Technical Requirement USL															
Technical Requirement LSL															

Functional Decomposition of Myoelectric Gripper with Sensory Feedback



APPENDIX B

US Digital S2 Rotary Optical Encoder Data Sheet

Features

- Small size
- Low cost
- 2-channel quadrature, TTL square wave outputs
- 3rd channel index option
- Tracks from 0 to 100,000 cycles/sec
- Ball bearing option tracks to 10,000 RPM
- -40 to +100C operating temperature
- Single +5V supply

	Supply Current	Output voltage low	Output voltage high	
Resolution	Typ / Max	Max	Min	Based on
2500 CPR, with index	55 / 57 mA	0.5 volts @ 8mA	2.0 volts @ -8mA	EM1

Pin-out

Pin	Description
1	Ground
2	Index
3	A channel
4	+5VDC power
5	B channel

Single Point Load Cell Specifications

Temp Effect:

Zero: $\pm 0.0022\%$ FS/ $^{\circ}$ F

Span: $\pm 0.0007\%$ rdg/ $^{\circ}$ F

Bridge Resistance: 350 Ω

Safe Overload: 150% rated capacity
(300% <6 kgf)

Ultimate Overload: 200% rated
capacity (400% <6 kgf)

Construction: Aluminum

Dimensions: Shown on page F-81

Cable: 0.6 m (26") 4-conductor cable

SPECIFICATIONS

Full Scale Output (User Must

Calibrate to Eliminate 10%

Tolerance): 2 mV/V $\pm 10\%$

(1 mV/V $\pm 10\%$ <6 kgf)

Excitation: 10 Vdc (15 Vdc max)

Non-Linearity: $\pm 0.015\%$ FS

(0.02% <6 kgf)

Hysteresis: $\pm 0.015\%$ FS

(0.02% <6 kgf)

Non-Repeatability: $\pm 0.02\%$ FS

Zero Balance: $\pm 5\%$ FS

Creep/Creep Recovery: 0.02% FS

Operating Temperature:

-10 to 50 $^{\circ}$ C (14 to 122 $^{\circ}$ F)

Compensated Temperature:

-10 to 50 $^{\circ}$ C (14 to 122 $^{\circ}$ F)

APPENDIX C

$$\sigma = \frac{M * y}{I} = \frac{39.375 * .375}{.00589} = 2506.9 \text{ psi}$$

Eq. D.1

$$\epsilon = \frac{\sigma}{E} = \frac{2506.9}{1 * 10^7} = .025\%$$

Eq. D.2

$$M = F * d = 22.5 \text{ lb} * 1.75 \text{ in} = 39.375 \text{ in.lb}$$

Eq. D.3

$$I = \frac{bh^3}{12} = \frac{.48 * .05^3}{12} = 5 * 10^{-6} \text{ in}^4$$

Eq. D.4

$$I_{\text{section}} = I + \text{area} * y^2 = .00589 \text{ in}^4$$

$$\text{area} = .024 \text{ in}^2, y = .35 \text{ in}$$

Eq. D.5

Figure D.1: Cross section of thinnest wall used to calculate maximum stress

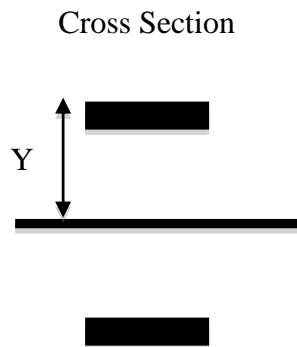
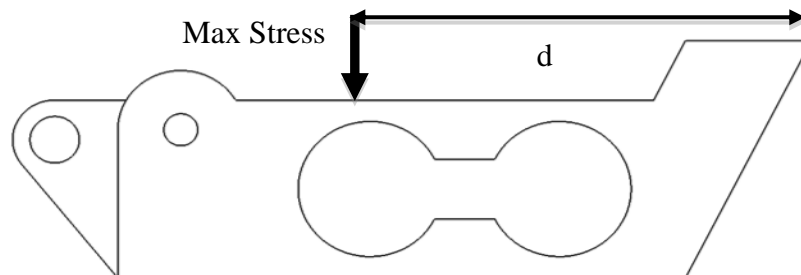
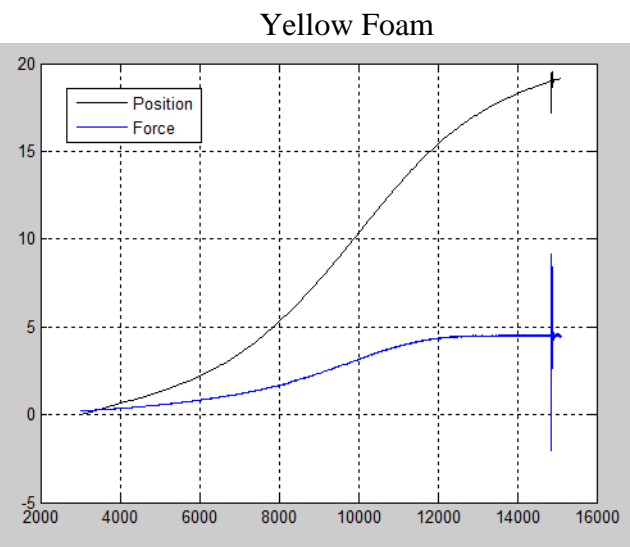
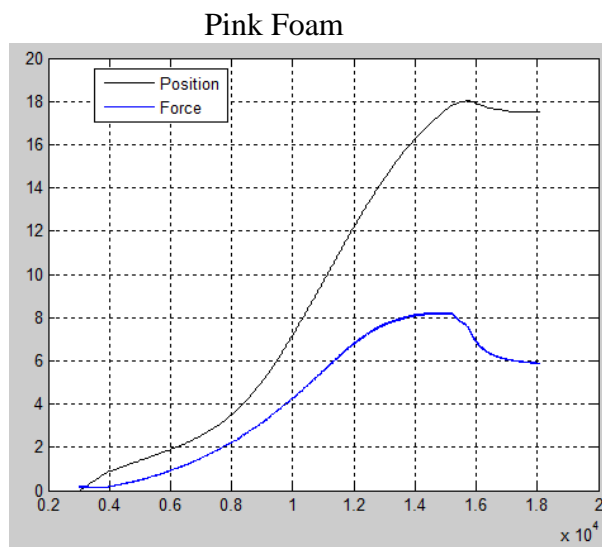
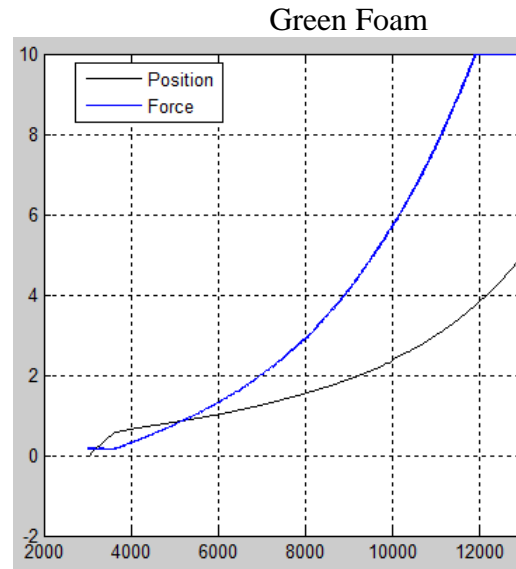
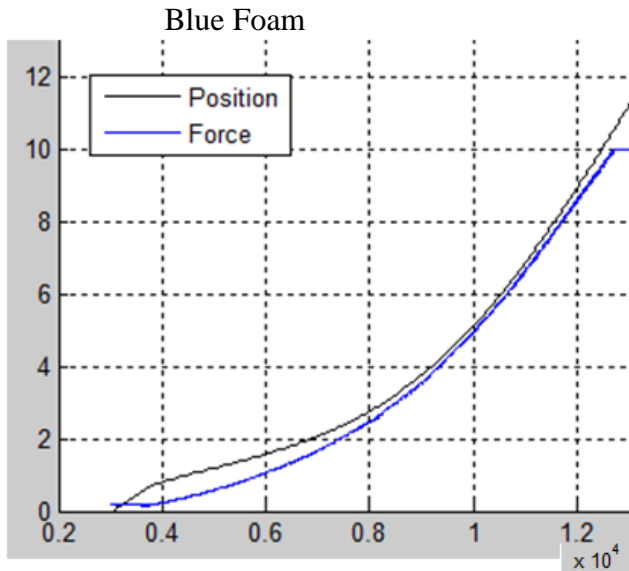


Figure D.2: Drawing of distance used to calculate moment for maximum stress calculations



Foam Calibration Results

Force [Volts] where [1V \approx 1 N]



Arduino Programming Code

```
#define ENCPINA_1 21 //PinA for gripper encoder
#define ENCPINB_1 20 // PinB for gripper encoder

// Declare variables
int openbutton = 50; // Open button located on digital Pin 50
int closebutton = 51; // Close button located on digital pin 51
int openbutton_value = 0; //Open button value. Initialized to 0
int closebutton_value = 0; //Close button value. Initialized to 0
int cmd = 0; //command signal sent to amplifier
int pwm = 13; //PWM signal
int emgsig = 1; //EMG signal Input connected to analog input pin 1
int emgground = 0; //EMG ground connected to analog input pin 0
int emgsig_value = 0; //EMG signal value initialized to 0
int emgground_value = 0; //EMG ground signal initialized to 0
int emgdiff = 0; //difference between EMG signal and EMG ground
int range = 168; //range of encoder signal
int low = 0; //lowest encoder reading
int high = 0; //highest encoder reading
int Pos = 0; //absolute encoder position based on high, low, and range

volatile int encPos_1 = 0; //relative gripper encoder position
volatile int encPos_1_last = 0; //previous encoder reading

// Initialize system
void setup() {
  pinMode(openbutton,INPUT); //declare pin 50 as digital input for openbutton
  pinMode(closebutton,INPUT); //declare pin 51 as digital input for closebutton
  pinMode(emgsig, INPUT); //declare pin 1 as analog input for EMG signal
  pinMode(emgground, INPUT); //declare pin 0 as analog input for EMG ground
  pinMode(pwm,OUTPUT); //declare pin 13 as pwm output

  pinMode(ENCPINA_1, INPUT); //declare pin 21 as digital input
  pinMode(ENCPINB_1, INPUT); //declare pin 21 as digital input

  digitalWrite(ENCPINA_1,HIGH);//initialize pin 21 as high
  digitalWrite(ENCPINB_1,HIGH);//initialize pin 20 as high

  attachInterrupt(2, readEncoderA_1, CHANGE);//declare pin 21 as interrupt 2 and define
  readEncoderA_1 as interrupt service routine
  attachInterrupt(3, readEncoderB_1, CHANGE);//declare pin 20 as interrupt 3 and define
  readEncoderB_1 as interrupt service routine

  Serial.begin(9600); //start serial connection
}
```

```

void loop()
{
  //Pushbutton Method
  cmd=100; // nominal value to stop motors, set according to pot too.
  openbutton_value = digitalRead(openbutton); //read openbutton pin
  closebutton_value = digitalRead(closebutton); //read closebutton pin

  if(openbutton_value == HIGH){
    cmd= 255;
  }
  if(closebutton_value == HIGH){
    cmd=0;
  }

  analogWrite(pwm,cmd);

  Pos = encPos_1-low;

  Serial.print(Pos);
  Serial.print("\t");
  Serial.print(encPos_1_last);
  Serial.print("\t");
  Serial.print(emgdiff);
  Serial.print("\n");

  encPos_1_last = encPos_1;
}

//Interrupt Service Routine for Channel A
void readEncoderA_1(){
  if(digitalRead(ENCPINA_1) ^ digitalRead(ENCPINB_1))
    encPos_1++;
  else
    encPos_1--;
}

//Interrupt Service Routine for Channel B
void readEncoderB_1(){
  if(digitalRead(ENCPINA_1) ^ digitalRead(ENCPINB_1))
    encPos_1--;
  else
    encPos_1++;
}

```

APPENDIX D

FX1901 OEM Compression Load Cell



- High Reliability Design for OEM, Appliance and Medical Applications
- 10 – 100 lbf Ranges
- Compact Coin Cell Package
- Anti-Rotation Mounting Features

FX1901 OEM Compression Load Cell

PERFORMANCE SPECIFICATIONS

Supply Voltage: 5.0V, Ambient Temperature: 25°C (unless otherwise specified)

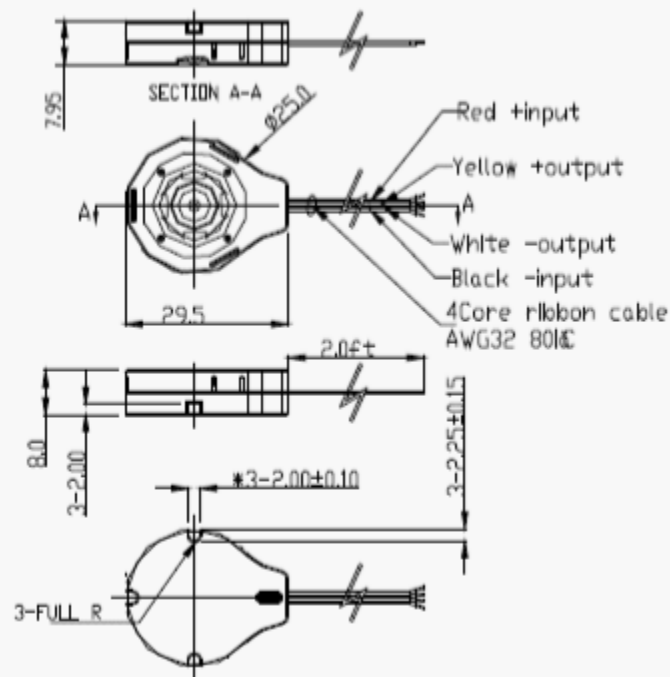
PARAMETERS	MIN	TYP	MAX	UNITS	NOTES
Span	16	20	24	mV/V	1
Zero Force Output		±15		mV	1
Accuracy (non linearity, hysteresis and repeatability)		±1		%Span	2
Input Resistance		3		kΩ	
Output Resistance		2.2		kΩ	
Temperature Error – Zero		±8		%Span	3
Temperature Error – Span		±2.5		%Span	3
Long Term Stability (1 year)		±1		%Span	
Maximum Overload			2.5X	Rated	
Compensated Temperature	0		50	°C	
Operating Temperature	0		50	°C	
Storage Temperature	-40		+85	°C	
Excitation Voltage	2	5	10	Vdc	
Isolation Resistance (250Vdc)	50			MΩ	
Deflection at Rated Load			0.05	mm	
Humidity	0		90	%RH	
Weight		8.1		grams	

For custom configurations, consult factory.

Notes

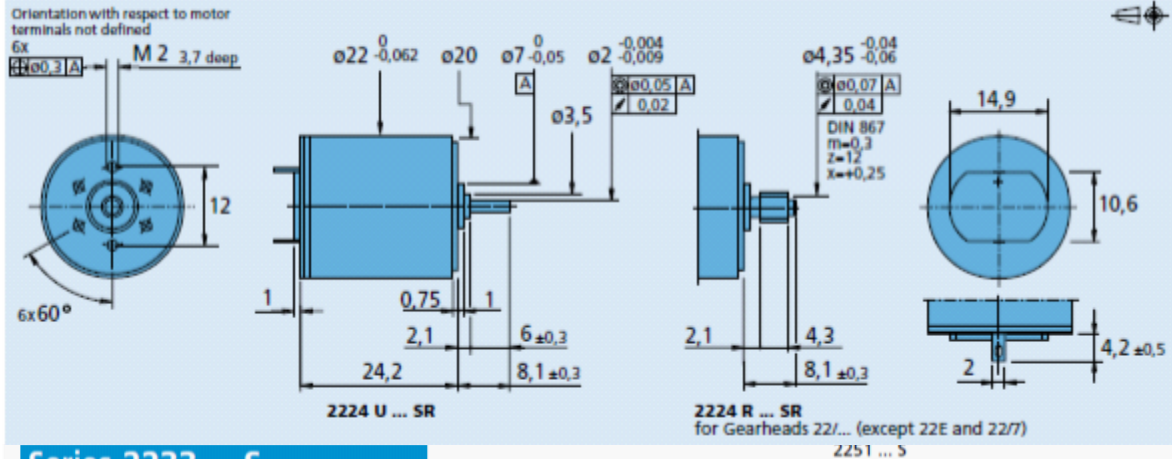
1. Ratiometric to supply.
2. Best fit straight line.
3. Maximum temperature error over compensated range with respect to 25°C.

DIMENSIONS



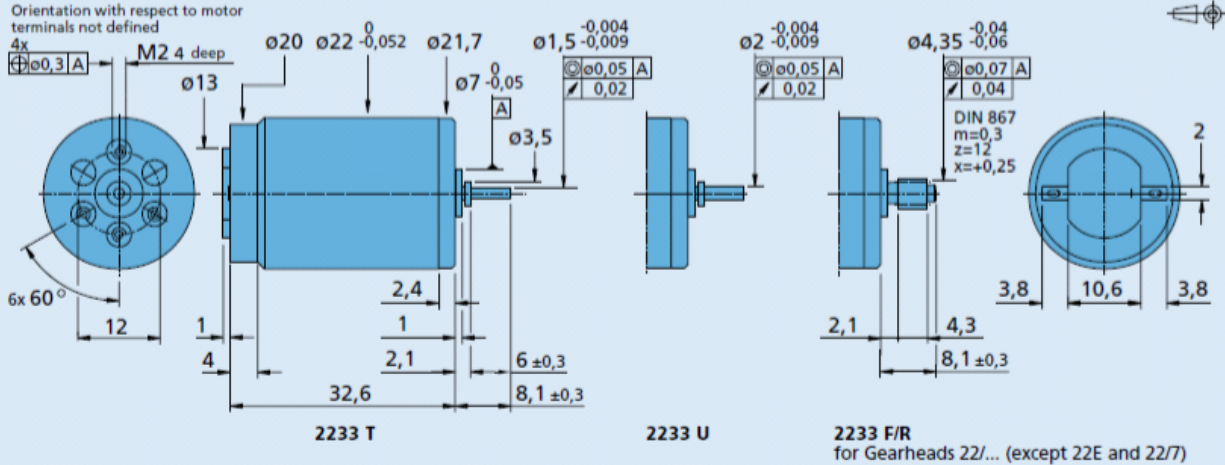
Series 2224 ... SR

		2224 U	003 SR	006 SR	012 SR	018 SR	024 SR	036 SR	
1	Nominal voltage	U_N	3	6	12	18	24	36	Volt
2	Terminal resistance	R	0,56	1,94	8,71	17,50	36,30	91,40	Ω
3	Output power	$P_{2 \max}$	3,92	4,55	4,05	4,54	3,88	3,46	W
4	Efficiency	η	80	82	82	82	81	80	%
5	No-load speed	n_0	8 100	8 200	7 800	8 100	7 800	7 800	rpm
6	No-load current (with shaft \varnothing 2,0 mm)	I_0	0,066	0,029	0,014	0,010	0,007	0,005	A
7	Stall torque	M_{st}	18,5	21,2	19,8	21,4	19,0	16,9	mNm
8	Friction torque	M_{fr}	0,23	0,2	0,2	0,21	0,2	0,22	mNm
9	Speed constant	k_n	2 730	1 380	657	454	328	219	rpm/V
10	Back-EMF constant	k_b	0,366	0,725	1,520	2,200	3,040	4,560	mV/rpm
11	Torque constant	k_{tw}	3,49	6,92	14,50	21,00	29,10	43,50	mNm/A
12	Current constant	k_i	0,286	0,144	0,069	0,048	0,034	0,023	A/mNm
13	Slope of n-M curve	$\Delta n / \Delta M$	438	387	394	379	411	462	rpm/mNm
14	Rotor inductance	L	11	45	200	450	800	1 800	μH
15	Mechanical time constant	τ_m	11	11	11	11	11	11	ms
16	Rotor inertia	J	2,4	2,7	2,7	2,8	2,6	2,3	gcm ²
17	Angular acceleration	α_{\max}	77	78	74	77	74	74	10 ³ rad/s ²
18	Thermal resistance	R_{th1} / R_{th2}	5 / 20						K/W
19	Thermal time constant	τ_{w1} / τ_{w2}	6,8 / 440						s
20	Operating temperature range:								
	- motor		- 30 ... + 85 (optional - 55 ... + 125)						°C
	- rotor, max. permissible		+ 125						°C
21	Shaft bearings		sintered bronze sleeves	ball bearings	ball bearings	ball bearings, preloaded			
22	Shaft load max.:		(standard)	(optional)	(optional)	(optional)			
	- with shaft diameter		2,0	2,0	2,0	2,0		mm	
	- radial at 3 000 rpm (3 mm from bearing)		1,5	8	8	8		N	
	- axial at 3 000 rpm		0,2	0,8	0,8	0,8		N	
	- axial at standstill		20	10	10	10		N	
23	Shaft play:								
	- radial	\leq	0,03	0,015	0,015	0,015		mm	
	- axial	\leq	0,2	0,2	0	0		mm	
24	Housing material		steel, black coated						
25	Weight		46						g
26	Direction of rotation		clockwise, viewed from the front face						



Series 2233 ... S

	2233 T	4.5 S	006 S	012 S	018 S	024 S	030 S		
1 Nominal voltage	U_N	4,5	6	12	18	24	30	Volt	
2 Terminal resistance	R	1,3	2,9	9,7	25,0	57,0	105	Ω	
3 Output power	$P_2 \text{ max.}$	3,85	3,06	3,66	3,18	2,47	2,08	W	
4 Efficiency	$\eta \text{ max.}$	86	85	84	82	80	79	%	
5 No-load speed	n_0	8 000	8 000	8 500	8 700	8 800	9 300	rpm	
6 No-load current (with shaft ϕ 1,5 mm)	I_0	0,020	0,013	0,009	0,007	0,005	0,004	A	
7 Stall torque	M_{Ht}	18,40	14,60	16,40	13,90	10,70	8,56	mNm	
8 Friction torque	M_{ft}	0,11	0,09	0,12	0,14	0,13	0,12	mNm	
9 Speed constant	k_n	1 790	1 340	714	488	371	314	rpm/V	
10 Back-EMF constant	k_E	0,559	0,745	1,400	2,050	2,690	3,180	mV/rpm	
11 Torque constant	k_M	5,34	7,12	13,40	19,60	25,70	30,40	mNm/A	
12 Current constant	k_i	0,187	0,141	0,075	0,051	0,039	0,033	A/mNm	
13 Slope of n-M curve	$\Delta n / \Delta M$	435	548	518	626	822	1 090	rpm/mNm	
14 Rotor inductance	L	70	130	400	600	1 600	2 200	μH	
15 Mechanical time constant	τ_m	12	11	12	14	11	12	ms	
16 Rotor inertia	J	2,60	1,90	2,20	2,10	1,30	1,10	gcm ²	
17 Angular acceleration	$\alpha \text{ max.}$	70	76	74	65	84	81	$\cdot 10^3 \text{ rad/s}^2$	
18 Thermal resistance	R_{th1} / R_{th2}	4 / 27						K/W	
19 Thermal time constant	τ_{w1} / τ_{w2}	4 / 660						s	
20 Operating temperature range:									
- motor		- 30 ... + 85 (optional - 55 ... + 125)							$^{\circ}\text{C}$
- rotor, max. permissible		+ 125							$^{\circ}\text{C}$
21 Shaft bearings		sintered bronze sleeves		ball bearings (optional)		ball bearings, preloaded (optional)			
22 Shaft load max.:		(standard)		(optional)		(optional)			
- with shaft diameter		1,5		2,0		2,0		mm	
- radial at 3 000 rpm (3 mm from bearing)		1,2		8		8		N	
- axial at 3 000 rpm		0,2		0,8		0,8		N	
- axial at standstill		20		10		10		N	
23 Shaft play:									
- radial	\leq	0,03		0,015		0,015		mm	
- axial	\leq	0,2		0,2		0		mm	



Series IE2 – 512

		IE2 – 64	IE2 – 128	IE2 – 256	IE2 – 512	
Lines per revolution	N	64	128	256	512	
Signal output, square wave		2				channels
Supply voltage	V _{DD}	4,5 ... 5,5				V DC
Current consumption, typical (V _{DD} = 5 V DC)	I _{DD}	typ. 6, max. 12				mA
Output current, max. ¹⁾	I _{OUT}	5				mA
Pulse width	P	180 ± 45				°e
Phase shift, channel A to B	Φ	90 ± 45				°e
Signal rise/fall time, max. (C _{LOAD} = 50 pF)	tr/tf	0,1 / 0,1				µs
Frequency range ²⁾ , up to	f	20	40	80	160	kHz
Inertia of code disc ³⁾	J	0,09				gcm ²
Operating temperature range		-25 ... +85				°C

¹⁾ V_{DD} = 5 V DC: Low logic level < 0,5 V, high logic level > 4,5 V: CMOS and TTL compatible

²⁾ Velocity (rpm) = f (Hz) x 60/N

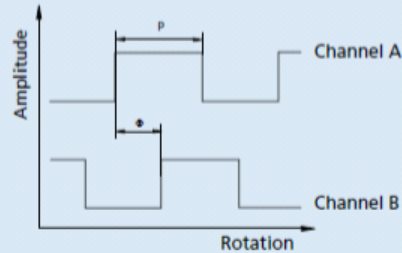
³⁾ For the brushless DC-Servomotors 1628 ... B, 2036 ... B and 2444 ... B the inertia of code disc is J = 0,14 gcm²

Ordering information

Encoder	number of channels	lines per revolution	in combination with:
IE2 – 64	2	64	DC-Micromotors series 1336 ... C, 1516 ... SR, 1524 ... SR, 1717 ... SR, 1724 ... SR, 1727 ... C, 2224 ... SR, 2232 ... SR, 2342 ... CR, 2642 ... CR, 2657 ... CR, 3242 ... CR, 3257 ... CR, 3863 ... C Brushless DC-Servomotors series 1628 ... B, 2036 ... B, 2057 ... B, 2444 ... B
IE2 – 128	2	128	
IE2 – 256	2	256	
IE2 – 512	2	512	

Output signals / Circuit diagram / Connector information

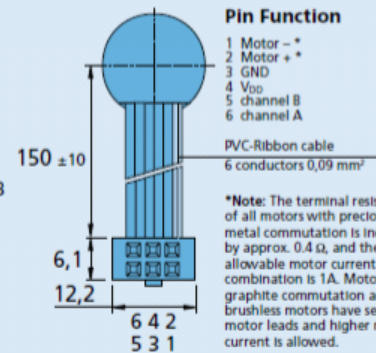
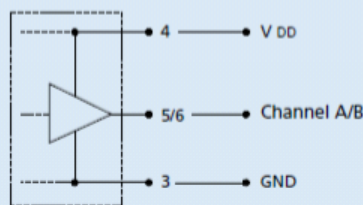
Output signals
with clockwise rotation as seen from the shaft end



Admissible deviation of phase shift:

$$\Delta\Phi = \left| 90^\circ - \frac{\Phi}{P} \times 180^\circ \right| \leq 45^\circ$$

Output circuit



Pin Function

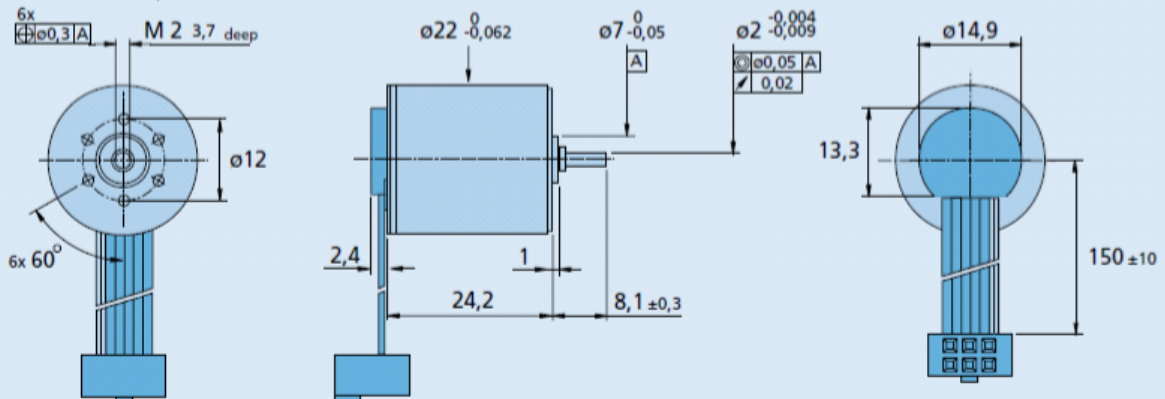
- 1 Motor -
- 2 Motor +
- 3 GND
- 4 V_{DD}
- 5 channel B
- 6 channel A

*Note: The terminal resistance of all motors with precious metal commutation is increased by approx. 0,4 Ω, and the max. allowable motor current in combination is 1A. Motors with graphite commutation and brushless motors have separate motor leads and higher motor current is allowed.

Connector
DIN-41651
grid 2,54 mm

DC-Micromotor 2224 U ... SR with Encoder IE2 – 16 ... 512

Orientation with respect to cable not defined



APPENDIX E
Bill of Materials:

Item	Qty	Source	Catalog #	Cost	Contact	Notes
Optical Encoder	1	US Digital	E4-360-157-d-d-d	\$33.50	usdigital.com	
Drive motor	1	Micromo	2224T012SRIE2-512	\$112.30	micromo.com	Includes magnetic encoder
Strain Gauge	25	Vishay	N2 N2K-13-T011Q-350/DP	\$125.00	Vishay.com	Minimum purchase is 25
Aluminum	1	McMaster-Carr	8975K429	\$13.09	mcmastercarr.com	L 12", W 4", H 0.5"
Socket head cap screws	3	McMaster-Carr	90128A245	\$11.12	mcmastercarr.com	1/4"-20 UNC SHCS minimum order is 50
Set Screw	1	McMaster-Carr	91375A242	\$13.19	mcmastercarr.com	10-32 UNC Set Screw minimum order is 100
Set Screw	1	McMaster-Carr	91375A143	\$8.62	mcmastercarr.com	6-32 UNC Set Screw minimum order is 100
Dowel Pins	1	McMaster-Carr	93600A147	\$8.42	mcmastercarr.com	5mm diam, 10mm long minimum order is 10

APPENDIX F

Material Selection Assignment (Functional Performance)

The purpose of this assignment is to show that proper techniques were used to select the proper materials for the two parts specified below.

Gripper load cell: The function and objective of the gripper load cell is to grip an object in a way that force is applied to the object at the gripper load cell contact point. One constraint that has been placed on the gripper load cell is it needs to withstand an applied force of 100 N without failure; a stiff light beam will be a good approximation. Also the material needs to be durable and light weight. We found the material index for our gripper load cell to be $\frac{E^{1/2}}{\rho} = C$ which is the minimum weight design of stiff beams, shafts and columns.

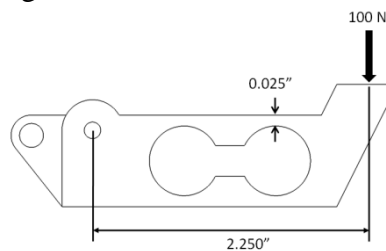


Figure F1. Free Body Diagram of Gripper Load Cell

For use as a material limit in CES we calculated the maximum stress using the equation for shear stress which was:

$$\sigma = \frac{My}{I}$$

To set a constraint in CES we used a shear stress limit to be > 17.24 MPa which was calculated in the initial stress / strain analysis section on page 18 of the report body. This combined with the machineability factor between 2 to 5, with 5 being the best, and the tree function where we were able to filter out any non metallic materials we found the following CES output graph shown in Figure F2.

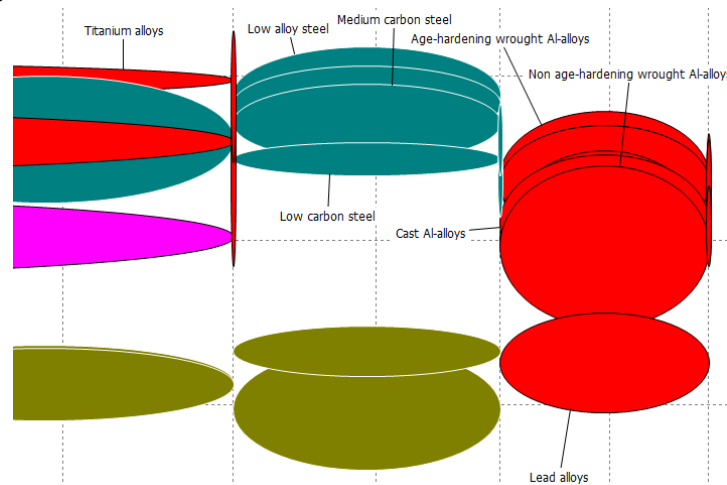


Figure F2. CES Output Graph for Gripper Load Cell

We chose to use T6061 Age Hardened Aluminum. The decision for this was economics, Professor Gillespie had enough of the material in his Haptix laboratory so we did not have to purchase any.

Gripper pivot shaft: The function and objective of the gripper pivot shaft is to provide a fulcrum point for the gripper load cell. One constraint that has been placed on the gripper pivot shaft is it needs to have a greater wear resistance than the aluminum it will be in contact with. We set the constraints to have a Vickers hardness $>$ 6061T Aluminum alloy ($>1.57e9$ Pa) and the yield strength $>$ the yield strength of 6061t Aluminum alloy ($>6.1e8$ Pa). Another limit we imposed on CES was the machinability factor, which we set to be between 2 to 5, with 5 being the best. The CES output graph can be seen in Figure F3.

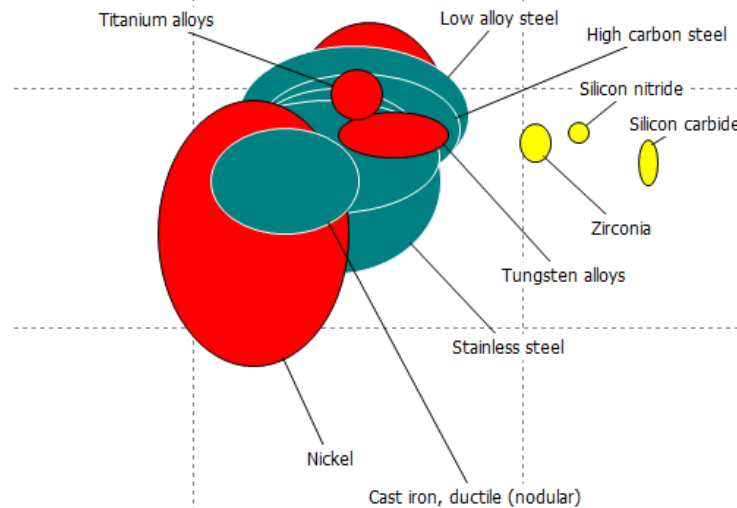


Figure F3. CES Output Graph for Gripper Pivot Shaft

We chose to use 1018 Low Alloy Steel to manufacture our gripper pivot shaft. We chose this as it is readily available from most supply stores and it is very low cost.

Material Selection Assignment (Environmental Performance)

SimaPro was used to calculate the environmental impact our material selection using the CES software would have when compared to one other similar material.

Gripper Load Cell:

It seems that the 6061 Aluminum Alloy was the better choice for overall pollution output. The Excel graph in Figure F4 shows air, water, raw materials, and waste pollution in kilograms.

Excel Bar Graph:

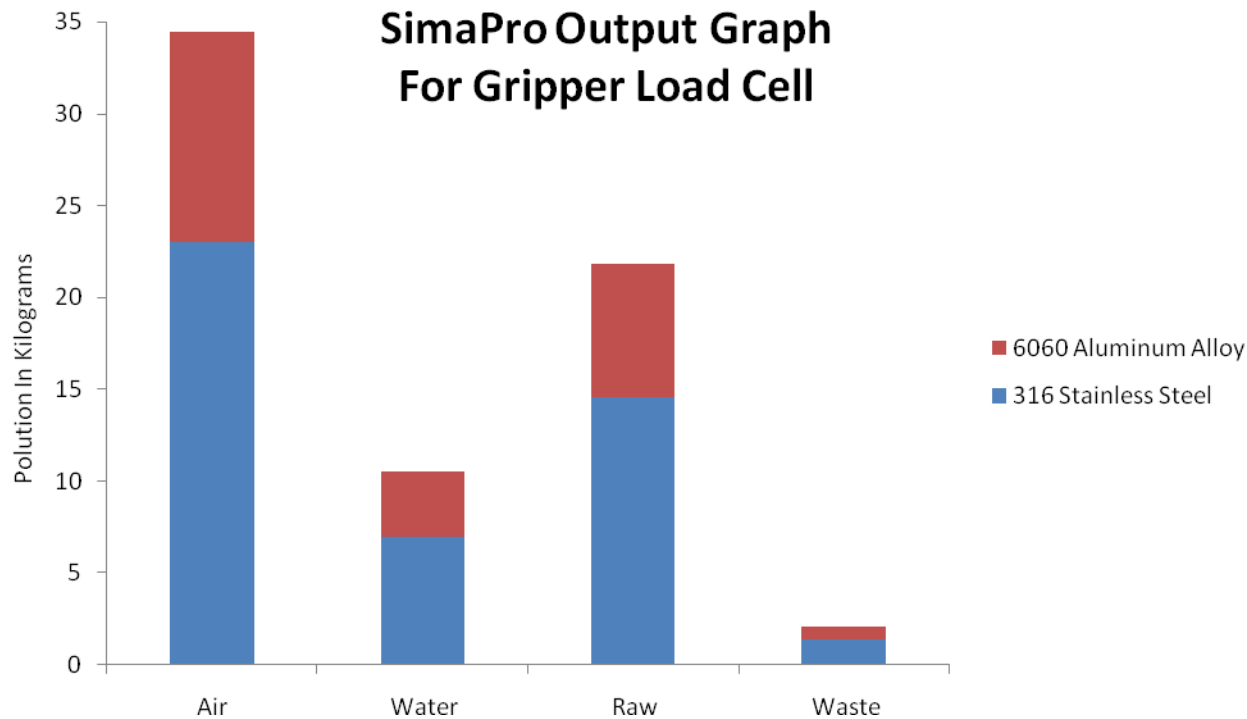
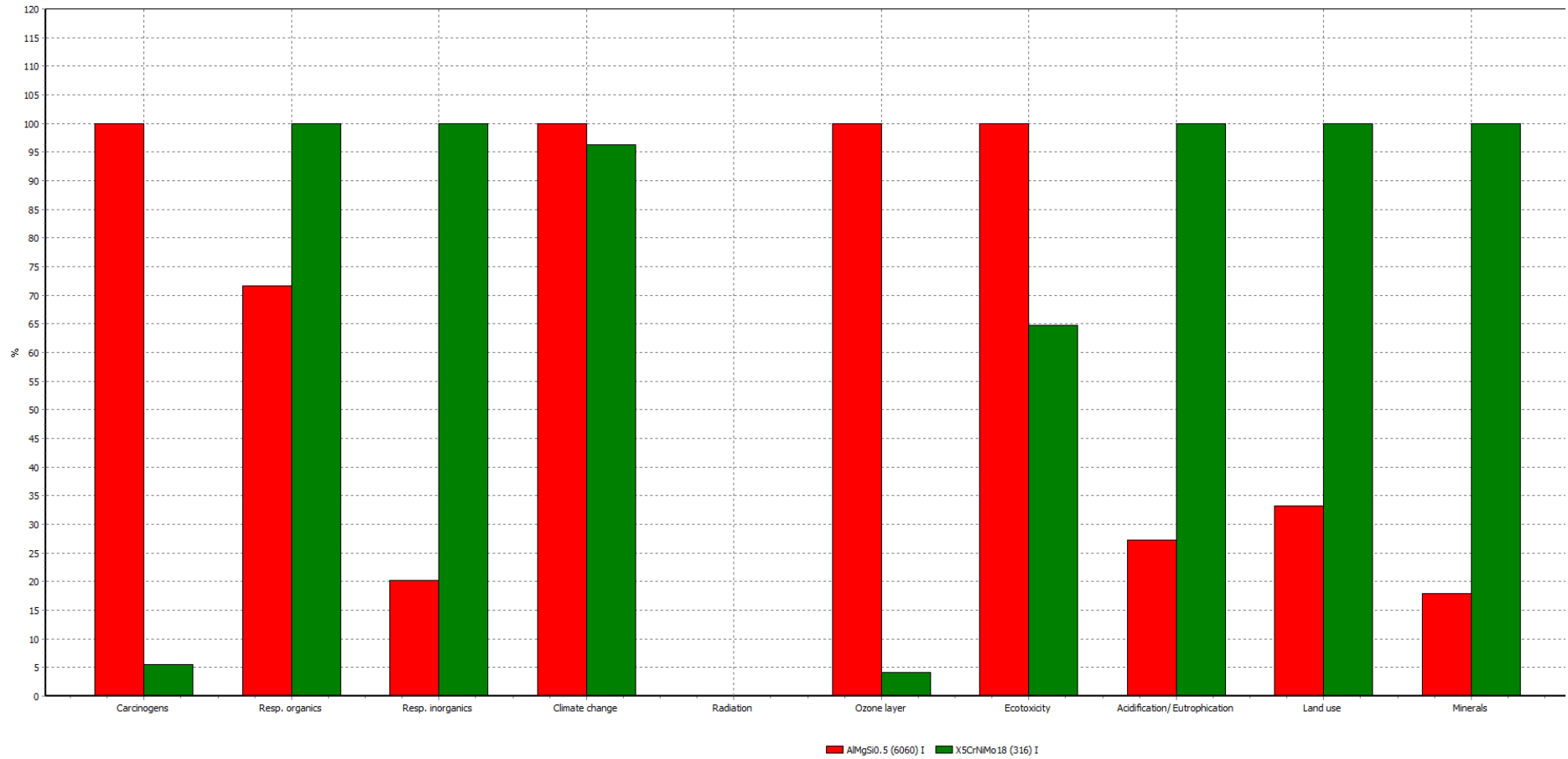


Figure F4. Total Mass of Emissions of Gripper Load Cell

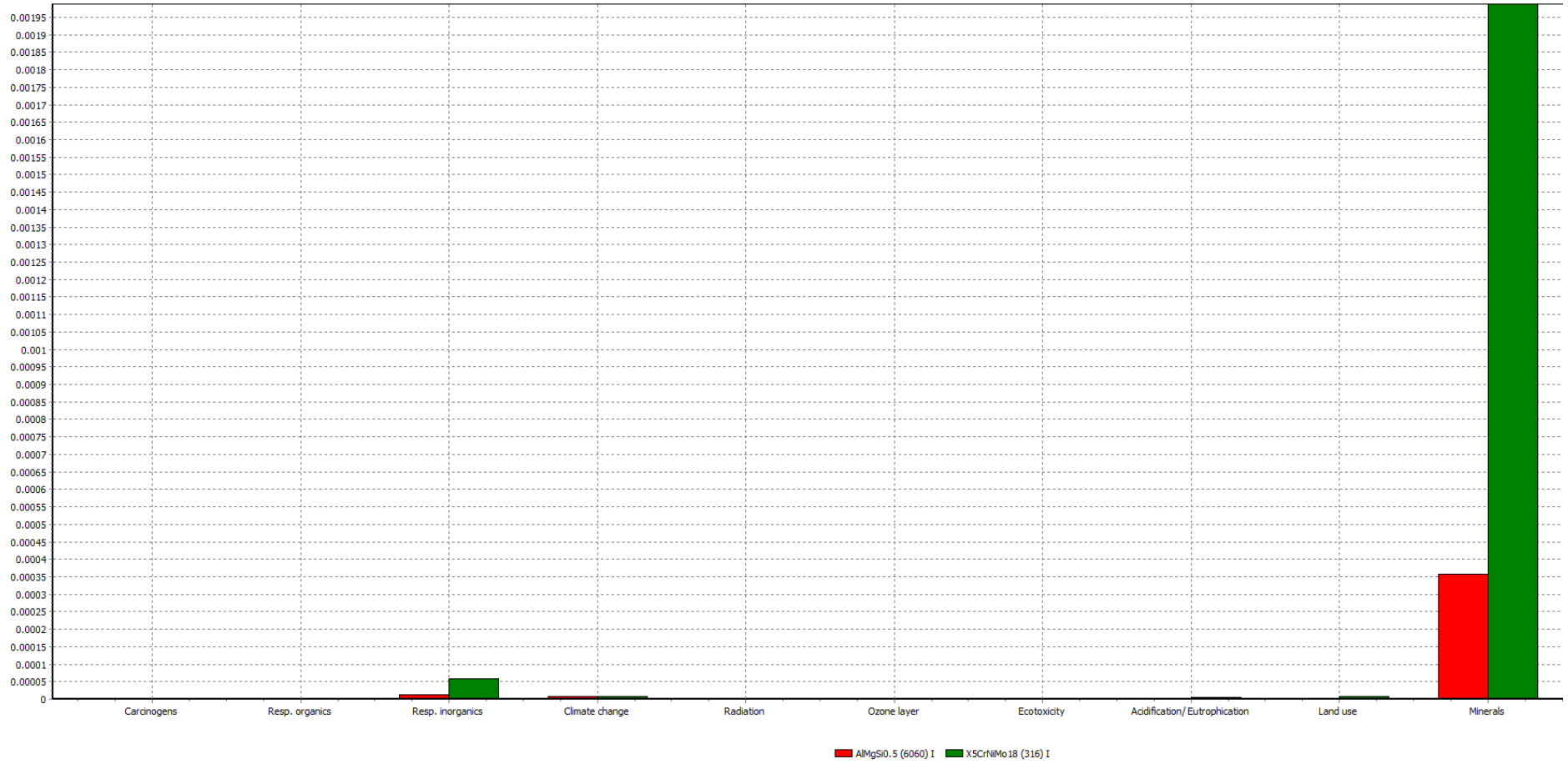
Impact Assessment: Characterization: From the characterization graph shown in Figure F5 several eco and human health factors are displayed. Both the 6061 Aluminum and the 316 Stainless Steel have an effect on human health and the environment.



Comparing 0.0617 lb AlMgSi0.5 (6060) I with 0.183 lb XScrNiMo18 (316) I; Method: Eco-indicator 99 (I) V2.02 / Europe ET 99 I/I / characterization

Figure F5. Impact on the Environment and Human Health

Impact Assessment: Normalization:



Comparing 0.0617 lb *AllMgSiO.5 (6060) I with 0.183 lb *X5CrNiMo18 (316) I; Method: Eco-indicator 99 (I) V2.02 / Europe EI 99 I/I / normalization

Impact Assessment: Single Score: From the single score graph shown in Figure F6 the 316 Stainless Steel has the highest impact on both the environment and to human health.

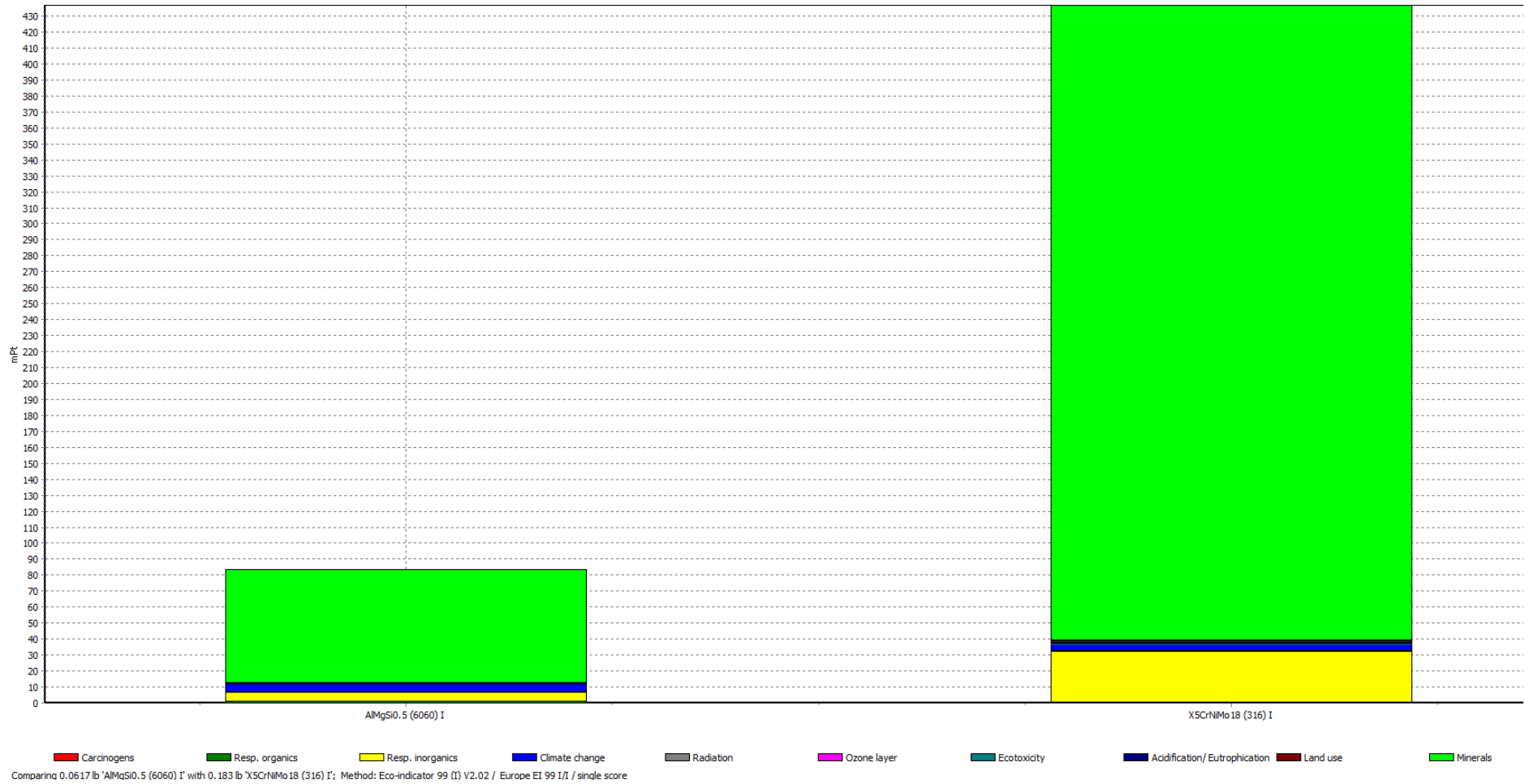


Figure F6. One to One Point Values

Gripper Pivot Shaft:

The following graphs include the SimaPro output graphs comparing the gripper pivot shaft when manufactured out of 1015 Low alloy Steel or 316 Stainless Steel. This bar graph denotes the SimaPro data that was collected showing the pollution output in kilograms of the Gripper pivot shaft clearly shows that the low alloy steel will have a smaller impact on the environment when compared with Stainless Steel.

Excel Bar Graph: The Excel graph in Figure F6 shows air, water, raw materials, and waste pollution in kilograms.

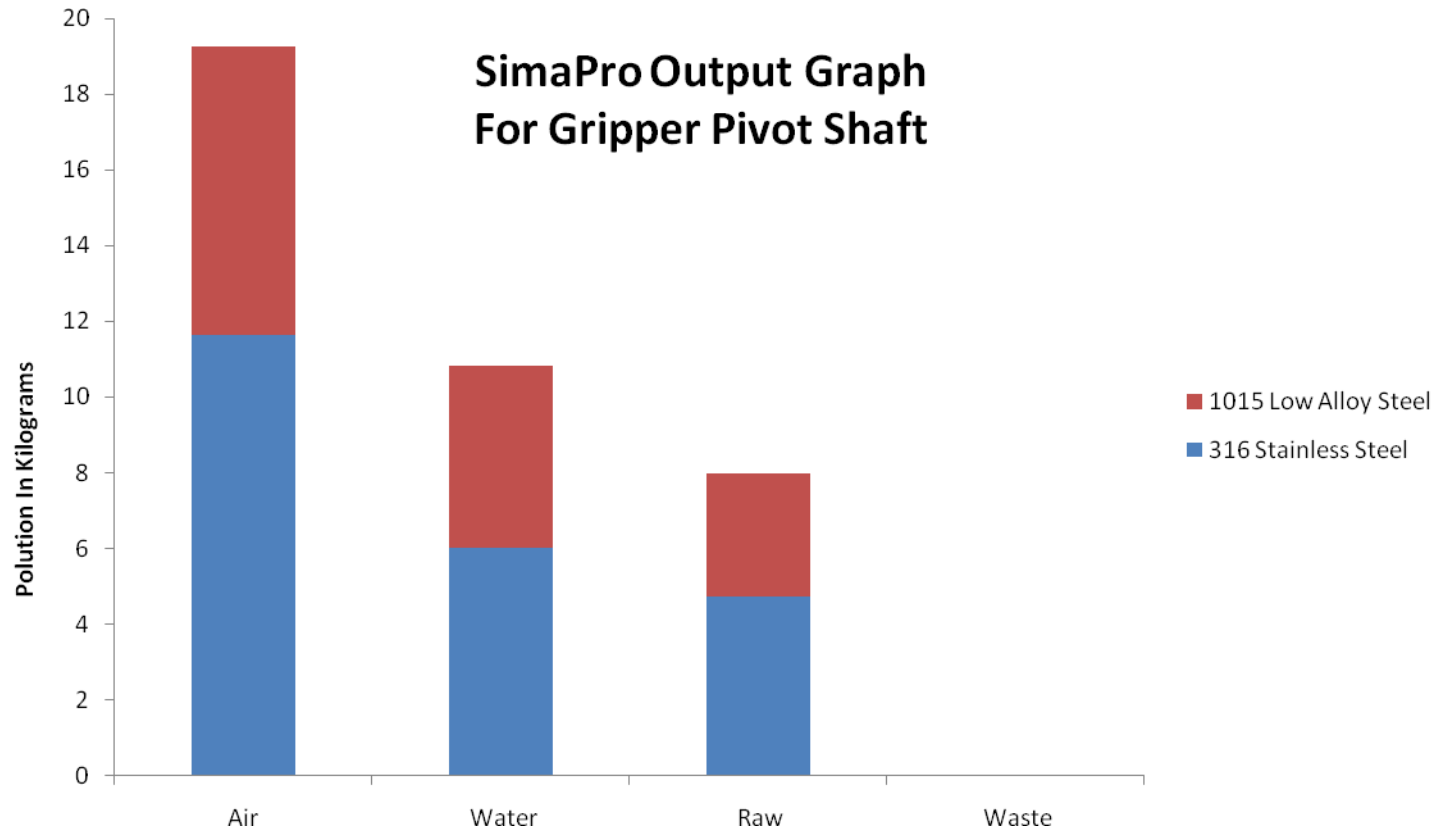
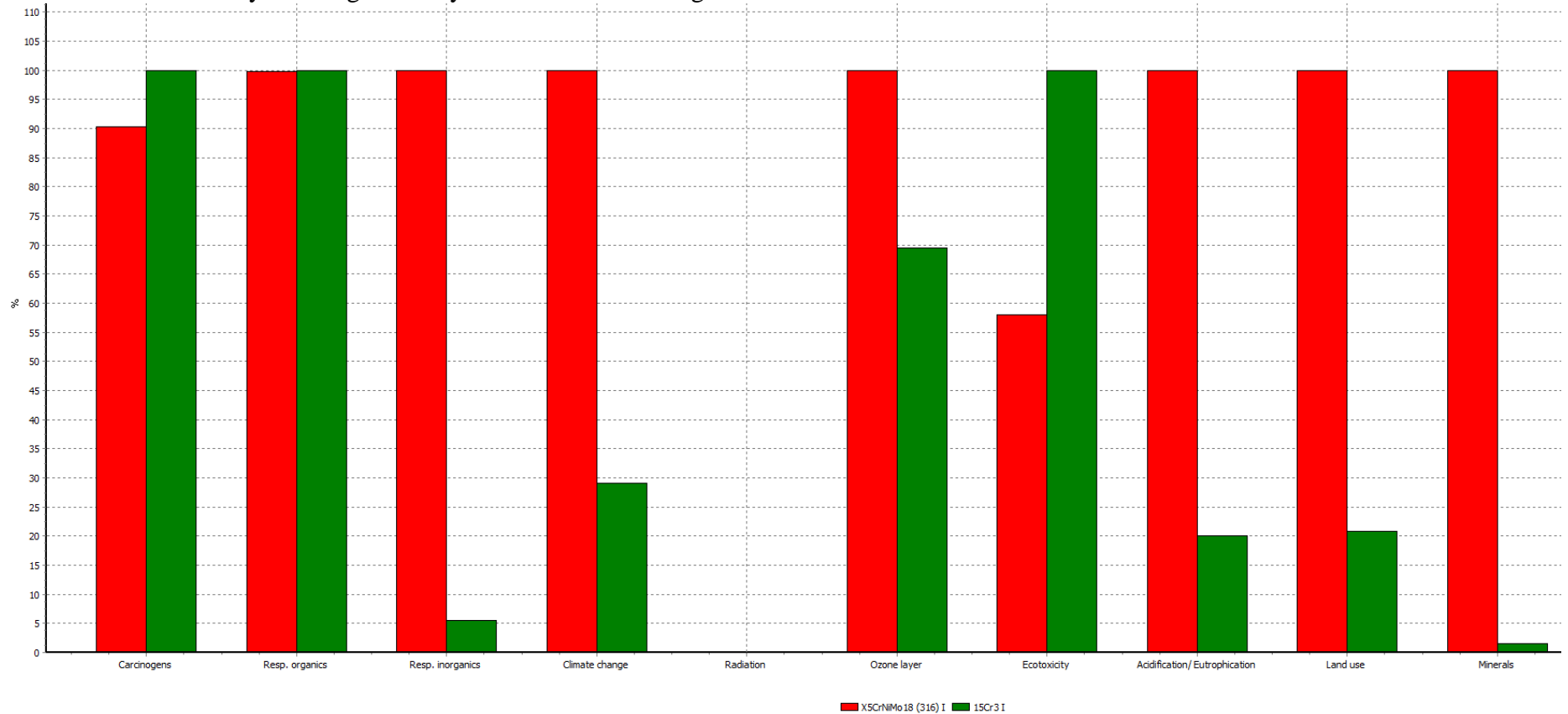


Figure F6. Total Mass of Emissions of Gripper Pivot Shaft

Impact Assessment: Characterization: From the characterization graph shown in Figure F7 several eco and human health factors are displayed. Both the 316 Stainless Steel and the 1015 Low Alloy Steel have an effect on human health and the environment with the 1015 Low Alloy Steel significantly lower in several categories.



Comparing 1 kg X5CrNiMo18 (316) I with 1 kg 15Cr3 I; Method: Eco-indicator 99 (I) V2.02 / Europe EI 99 I/I / characterization

Figure F7. Impact on the Environment and Human Health

Impact Assessment: Normalization



■ X5CrNiMo18 (316) I ■ 15Cr-3 I

Comparing 1 kg 'X5CrNiMo18 (316) I' with 1 kg '15Cr-3 I'; Method: Eco-indicator 99 (I) V2.02 / Europe EI 99 I/I / normalization

Impact Assessment: Single Score: From the single score graph shown in Figure F8 the 316 Stainless Steel has the highest impact on both the environment and to human health.

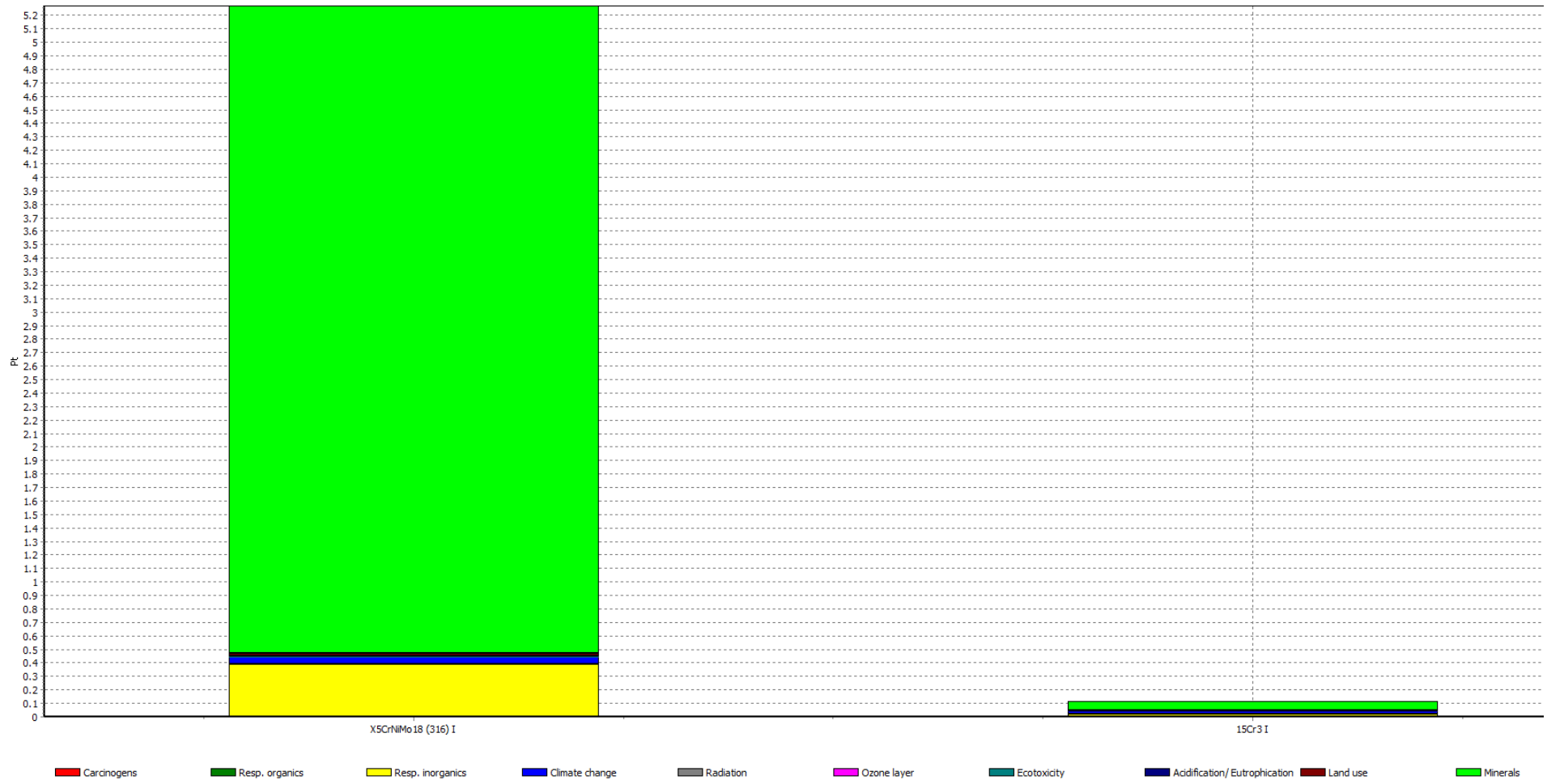


Figure F8. One to One Point Values

Manufacturing Process Selection Assignment

Real World Production Volume: According to the Amputee Coalition of America (http://www.amputee-coalition.org/nllc_faq.html#2.) there are currently 1.7 million amputees living in the United States. In 2007 there were 185,000 amputations. From these numbers we could reasonably be producing up to 10,000 units per year in the United States alone if our design becomes marketable.

The material selected for the Gripper load cell seems to be the appropriate choice for the manufacturing needs of our estimated production number. The 6061 Aluminum alloy has a more than adequate strength and will also resist corrosion. The 6061 Aluminum alloy also has a high machineability as can be seen from Figure F2. From the environmental study that was completed using the SimaPro software it was found that the 6061 Aluminum alloy had lower adverse environmental and health risks as can be seen in the SimaPro single score output graph in Figure F6.